

Interannual to Decadal Predictability of Tropical and North Pacific Sea Surface Temperatures

Matthew Newman

CIRES Climate Diagnostics Center, University of Colorado, and Physical Sciences
Division/NOAA Earth System Research Laboratory, Boulder, Colorado

Email: matt.newman@noaa.gov

Submitted to *Journal of Climate*

Revised Thursday, July 27, 2006

ABSTRACT

A multivariate empirical model is used to show that predictability of annual mean SST in both the tropical and North Pacific oceans is mostly limited to a few years, despite the presence of spectral peaks on decadal timescales. The model used is a linear inverse model (LIM) derived from the observed simultaneous and one-year lag correlation statistics of July-June averaged SST from the Hadley Centre Global Sea Ice and Sea Surface Temperature (HadISST) dataset for the years 1900-2002. The model accurately reproduces the power spectra of the data, including interannual and interdecadal spectral peaks that are significant relative to univariate red noise. Eigenanalysis of the linear dynamical operator yields propagating eigenmodes that correspond to these peaks but have very short decay times and thus limited predictability. What long-term predictability exists appears due to two stationary eigenmodes, one similar to the 1900-2002 trend and the other representing multidecadal fluctuations. Predictability of these two stationary eigenmodes is significantly enhanced by tropical-North Pacific coupling. Neither stationary eigenmode is well captured in the control run of any coupled GCM in the CMIP project of the IPCC Fourth Assessment Report (AR4), perhaps because in all the GCMs tropical SST decadal variability is too weak and North Pacific SSTs are too independent of the Tropics.

A key implication of this analysis is that the Pacific Decadal Oscillation (PDO) may represent not a single phenomenon but rather the sum of several processes, each of which represent different spatial patterns whose temporal evolution can be separately modeled as red noise with differing autocorrelation timescales. The sum of these red noises can give rise to apparent PDO “regime shifts” and seeming characteristics of a long memory

process. Such shifts are not predictable beyond the timescale of the most rapidly decorrelating noise, less than two years. Both the expected duration of regimes, and multidecadal variation in the correlation of the PDO with the Tropics, depend upon the relative amplitudes of different eigenmodes and need not reflect any change in underlying dynamics.

1 Introduction

Predictability of the atmosphere on annual to decadal timescales comes primarily from the ocean. Observations of spectral peaks on these timescales in both the North Pacific and Tropical IndoPacific oceans, particularly from long-term proxy data (Evans et al 2001; Biondi et al 2001; D'Arrigo et al. 2001; Gedalof et al. 2002; D'Arrigo et al. 2006), as well as modeling studies of oceanic dynamics acting on multiyear timescales (Venzke et al. 2000; Schneider and Miller 2001; Schneider et al. 2002; Scott and Qiu 2003), suggest some decadal (or at least greater than interannual) oceanic predictability may exist. In addition, there has been much interest in so-called “regime shifts” in the climate system, conspicuously rapid transitions between relatively stable atmospheric and oceanic states that appear to occur roughly every few decades (e.g., Trenberth and Hurrell 1994; Hare and Mantua 2000) and perhaps drive similar changes in marine ecosystems (e.g. Miller et al. 1994; Mantua et al. 1997; Benson and Trites 2002; Miller et al. 2004).

A key unresolved question has been how North Pacific sea-surface temperature (SST) predictability is affected by mechanisms of decadal variability “internal” to the extratropics, versus mechanisms driven from the Tropics and/or that drive the Tropics. Many modeling studies consider the North Pacific in isolation, where extratropical atmospheric variability that is temporally incoherent but spatially coherent drives both a local SST response due to anomalous surface fluxes and Ekman advection, and a remote SST response in the Kuroshio-Oyashio extension region¹ due to oceanic Rossby waves. Multi-decadal spectral peaks in this view are then due to stochastically forced spatial

¹ Qiu (1995) shows observational evidence indicating that the Kuroshio and Oyashio extensions are separate at high resolution.

resonance and/or to coupled air-sea feedback (Frankignoul et al. 1997; Jin 1997; Saravanan and McWilliams 1998; Weng and Neelin 1999; Seager et al. 2001; Schneider et al. 2002). Observational analyses have identified patterns that statistically explain much SST variability (e.g., Deser and Blackmon 1995; Zhang et al. 1997; Mantua et al. 1997; Livezey and Smith 1999; Tourre et al. 1999; Deser et al. 2004; An and Wang 2005), finding some “modes” of North Pacific SST variability that appear related to the Tropics and some that do not. In general, however, limitations of the statistical analyses make dynamical interpretation unclear, especially concerning disentangling tropical influences from purely internal North Pacific dynamics.

That there is at least some tropical influence upon North Pacific decadal variability seems clear (Trenberth and Hurrell 1994; Zhang et al. 1997; Evans et al. 2001; Newman et al. 2003b; Seager et al. 2004). For leads of a few months, the dominant mode of tropical SST variability, El Niño-Southern Oscillation (ENSO), is highly correlated year-round with the dominant mode of North Pacific variability, the Pacific Decadal Oscillation (PDO), as a result of the atmospheric bridge (Alexander et al. 2002). Because of wintertime re-emergence (Alexander et al. 1999), North Pacific SSTs also have year-to-year memory. Thus, a simple model of the PDO-ENSO relationship can be constructed (Newman et al. 2003b; hereafter NCA) showing that, just as the ocean acts to redden atmospheric noise (Frankignoul and Hasselmann 1977), it also acts to redden the ENSO signal. That is, the observed spatial pattern of Pacific SST decadal variability, with relatively higher amplitude in the extratropics than in the Tropics, should be at least partly a consequence of a reddened ENSO response (NCA).

Although useful conceptually, the NCA model is limited by its simplicity. For example, the univariate approach restricts representation of Tropical and North Pacific SST anomalies to a single pattern each. However, North Pacific variability is not equally sensitive to all parts of the Tropics (e.g., Alexander et al. 2002; Barsugli and Sardeshmukh 2002), and decadal variability within the Tropics does not coincide precisely with interannual variability (Zhang et al. 1997; Deser et al 2004). Decadal variability in the North Pacific is not represented by the PDO alone (Deser and Blackmon 1995; Nakamura et al. 1997; Bond et al. 2003) and interactions between different parts of the basin are important on decadal timescales (Schneider and Cornuelle 2005). Thus a multivariate analysis is clearly preferable.

Another key limitation of the NCA model is that it assumes a perfect forecast of ENSO, a restriction that would be preferable to relax, especially since it is possible that the North Pacific is not merely forced by the Tropics but may force the Tropics and/or be coupled to it (Gu and Philander 1997; Barnett et al 1999; Schneider et al 1999; Vimont et al. 2001, 2003; Solomon et al 2003). Thus, to investigate variability and predictability of the North Pacific, the Tropics must be included as part of the system, not external to it.

To extend the NCA analysis, we will apply linear inverse modeling (LIM) to a state vector constructed from Tropical and North Pacific SSTs. LIM attempts to empirically extract the linear dynamical system from simultaneous and time-lag covariance statistics of the system variables, and has been successfully used in geophysical contexts ranging from subseasonal atmospheric variability (Winkler et al. 2001; Newman et al. 2003a) to seasonal ENSO dynamics and prediction (Penland and Matrosova 1994; Penland and Sardeshmukh 1995; Penland 1996). LIM may be simply considered as a multivariate

analogue to the univariate red noise null hypothesis for SST variability first proposed by Frankignoul and Hasselman (1977). Unlike its univariate counterpart, however, multivariate red noise can have transient anomaly growth and both stationary and propagating anomalies, and thus spectral peaks (e.g., Penland and Sardeshmukh 1995). Also, predictability estimates from LIM are straightforward and can be understood from fundamental aspects of the linear system (Newman et al. 2003a; Chang et al. 2004).

The outline of the paper is as follows. Multivariate red noise and linear inverse modeling are discussed in section 2, and section 3 describes details of data and model. In section 4, the LIM constructed from 102 years of SST data is shown to reproduce the power spectra of the leading PCs, and it is also found that for forecast leads greater than one year most LIM forecast skill results from two stationary eigenmodes of the linear operator. Effects of tropical-extratropical coupling are investigated in section 5, and our analysis is applied to the output of 18 coupled GCMs in section 6, where it is suggested that the GCMs significantly underestimate tropical forcing of the North Pacific on both interannual and interdecadal timescales. Concluding remarks are in section 7.

2 Multivariate red noise and linear inverse modeling

2.1 A multivariate null hypothesis

A standard approach to analyzing long-term datasets is to look for spectral “peaks” above a univariate red noise background. That is, one assumes a null hypothesis for a time series x :

$$1) \quad \frac{dx}{dt} = lx + \xi$$

where $l < 0$, $-1/l$ is the decorrelation timescale and ξ represents white noise. Predictability of x is limited by l . Such a simple null hypothesis is often hard to beat; for example, monthly time series of the leading North Pacific pattern of both SST (Pierce 2001; Rudnick and Davis 2003) and sea level pressure (Percival et al. 2001) cannot be distinguished from univariate red noise at the 95% confidence level. In addition, from a SST prediction standpoint, atmospheric variability might as well be random, since the atmosphere varies so rapidly it cannot be predicted on the much longer dynamical timescales of the ocean. This natural timescale separation justifies the simple approximation (1) in which the ocean integrates forcing by weather approximated as white noise (Hasselmann 1976; Frankignoul and Hasselmann 1977), a picture perhaps only slightly modified by air-sea coupling (Barsugli and Battisti 1998).

The concept underlying this approximation can be usefully extended to the more general case of multivariate nonlinear dynamics. That is, a timescale separation between “slow” dynamics and “fast,” or rapidly varying, nonlinearities can be shown to allow the approximation of a multivariate nonlinear tendency equation for a state vector \mathbf{x} as

$$2) \quad \frac{d\mathbf{x}}{dt} = \mathbf{L}\mathbf{x} + \xi ,$$

the sum of stable and predictable linear dynamics plus unpredictable white noise ξ (e.g., Papanicolaou and Kohler 1974; Hasselmann 1976; see also Penland 1996). [Note that for the problem considered in this paper, noise represents not only atmospheric variability but more generally any other rapidly decorrelating nonlinearity.] Put simply, variability is modeled as *multivariate* red noise. However, since the linear operator \mathbf{L} is a matrix its dynamics are represented by the eigenanalysis $\mathbf{L}\mathbf{u}_j = \mathbf{u}_j \lambda_j$, where \mathbf{u}_j are the eigenmodes

and λ_j are the corresponding eigenvalues that may be complex. This results in two critical differences between univariate and multivariate red noise. First, complex eigenvalues correspond to propagating eigenmodes with defined periods. Second, although all the eigenvalues are damped (that is, they have negative real parts), in most geophysical systems of interest \mathbf{L} is nonnormal, so that the eigenvectors are not orthogonal and thus transient anomaly growth is possible (e.g., Farrell 1988). Since \mathbf{L} is stable, an energy balance relationship called a fluctuation-dissipation relationship can be derived from (2):

$$3) \quad \mathbf{L}\mathbf{C}_0 + \mathbf{C}_0\mathbf{L}^T + \mathbf{Q} = 0,$$

where $\mathbf{C}_0 = \langle \mathbf{x}(0)\mathbf{x}(0)^T \rangle$ is the zero-lag covariance matrix and \mathbf{Q} is the noise covariance matrix which can have non-zero off-diagonal elements.

2.2 *Linear inverse modeling*

Obviously, not all nonlinear dynamical systems can be usefully represented by (2) (e.g., Penland 1989). Two approaches to determine if (2) is a good approximation are the “forward” and “inverse” methods. For the forward method, one might try to rewrite the physical equations in the form of (2). Such a derivation is likely extremely difficult for the full climate system. Alternatively, from (2),

$$4) \quad \mathbf{C}_\tau = \exp(\mathbf{L}\tau)\mathbf{C}_0 = \mathbf{G}(\tau)\mathbf{C}_0$$

where $\mathbf{C}_\tau = \langle \mathbf{x}(\tau)\mathbf{x}(0)^T \rangle$ is a time-lag covariance matrix at some lag τ . This suggests an inverse method, in which (given enough good data) \mathbf{L} , as well as \mathbf{Q} , can be estimated from observed \mathbf{C}_τ and \mathbf{C}_0 for some specified lag $\tau=\tau_0$, as described for example in Penland and Sardeshmukh (1995). An effectively linear, stochastically forced model of a

system thus constructed is called a Linear Inverse Model (LIM) (Penland 1989; Penland and Ghil 1993; Penland 1996; Delsole and Hou 1999; Johnson et al. 2000; Winkler et al. 2001; Newman et al. 2003a). In principle, \mathbf{L} obtained through LIM should be identical to \mathbf{L} obtained from the forward method.

Whether the LIM is a good representation of the data is tested a posteriori, as described in the above-cited references. Here we stress one important point. If the dynamics of \mathbf{x} are effectively linear, it should not matter what lag τ_0 is used to determine \mathbf{L} . That is, $\mathbf{C}_{\tau_1} = \exp(\mathbf{L}\tau_1)\mathbf{C}_0$ and $\mathbf{C}_{\tau_2} = \exp(\mathbf{L}\tau_2)\mathbf{C}_0$. The simplest test of LIM is to determine \mathbf{L} from many different lags and then compare each \mathbf{L} . Unfortunately, if the “true” \mathbf{L} has some relatively high-frequency eigenmodes, then lags τ that are about an eigenmode half-period cannot be used to determine \mathbf{L} , even though $\mathbf{G}(\tau)$ can be determined. This “Nyquist problem” (Penland and Sardeshmukh 1995) occurs for all linear dynamical systems, so it does not necessarily invalidate the assumption of linearity. An alternative test is to determine if \mathbf{L} , determined at one shorter lag τ_0 , reproduces the observed autocorrelation of \mathbf{x} at all longer lags from (4) (Winkler et al. 2001; Newman and Sardeshmukh 2006). In this paper, we will employ the related calculation wherein observed power spectra of \mathbf{x} are compared to those predicted by LIM.

2.3 *Estimating predictability from LIM*

LIM results in straightforward predictability estimates (Newman et al. 2003a). Briefly, given (2), forecasts made for lead τ are

$$5) \quad \hat{\mathbf{x}}(t + \tau) = \mathbf{G}(\tau) \mathbf{x}(t).$$

LIM forecast errors $\mathbf{e}(t + \tau) = \mathbf{x}(t + \tau) - \hat{\mathbf{x}}(t + \tau)$ are random and have covariance $\mathbf{E}(\tau) = \mathbf{C}_0 - \mathbf{G}(\tau)\mathbf{C}_0\mathbf{G}^T(\tau)$. Forecast skill measured by the average anomaly correlation $\rho(\tau)$ between forecast and verification anomalies is a function of S , the forecast signal-to-noise ratio, as

$$6) \quad \rho(\tau) = \frac{S}{[1 + S^2]^{1/2}}$$

(Sardeshmukh et al. 2000). The LIM assumes noise is independent of the state; so on average higher forecast skill is directly related to stronger predictable signal (Newman et al. 2003a). Therefore, long-range forecasts have highest skill for relatively large initial amplitude in the least-damped eigenmodes of \mathbf{L} .

3 Model details and data

3.1 SST data and EOF analysis

The dataset used was essentially the same as used by NCA. SSTs were from the Hadley Sea Ice and Sea Surface Temperature analysis (HadISST; Rayner et al. 2003) for the years 1900–2002. Similar calculations with Kaplan SST data (Kaplan et al. 1998; not shown) gave qualitatively similar results. The data were averaged into 5x5 degree gridboxes. Data were averaged into annual means extending from July through June of the following year. Anomalies were determined by removing the 1950/51–2001/02 climatological annual mean. Empirical orthogonal functions (EOFs) were determined for the same period, and then earlier data were projected onto these patterns to produce 102 yr time series for each EOF. NCA determined EOFs from monthly data and then took a July-June mean of the resulting time series, but this made very little difference in our

analysis. Prior to 1950, the general paucity of data may make difficult a determination of dynamics on seasonal timescales, but HadISST annual means for that period appear dynamically relevant (Rayner et al. 2003). NCA showed that using a July-June mean might avoid some seasonality issues for tropical variability, North Pacific variability, and the tropical-North Pacific relationship. However, seasonality is likely still relevant to decadal variability (Vimont 2005).

EOFs were determined separately for the Tropics (20°S-20°N and 60°E-60°W) and the North Pacific (21°N-60°N). The three leading EOFs for each field are shown in Fig. 1. Annual averages reduce the number of degrees of freedom, so few EOFs are needed to explain a significant fraction of variance of either field. The leading EOFs dominate the variability of their respective fields and are typically named “ENSO” and the “PDO.”

3.2 Construction of LIM

The SST state vector is

$$7) \quad \mathbf{x} = \begin{bmatrix} \mathbf{x}_N \\ \mathbf{x}_T \end{bmatrix},$$

where \mathbf{x}_N is anomalous North Pacific SST and \mathbf{x}_T is anomalous Tropical SST, so that (2) becomes

$$8) \quad \frac{d\mathbf{x}}{dt} = \frac{d}{dt} \begin{bmatrix} \mathbf{x}_N \\ \mathbf{x}_T \end{bmatrix} = \begin{bmatrix} \mathbf{L}_{NN} & \mathbf{L}_{NT} \\ \mathbf{L}_{TN} & \mathbf{L}_{TT} \end{bmatrix} \begin{bmatrix} \mathbf{x}_N \\ \mathbf{x}_T \end{bmatrix} + \begin{bmatrix} \boldsymbol{\xi}_N \\ \boldsymbol{\xi}_T \end{bmatrix}.$$

Here $\boldsymbol{\xi}_N$ and $\boldsymbol{\xi}_T$ are white noise forcings of \mathbf{x}_N and \mathbf{x}_T , respectively. Note that separating Tropical and North Pacific SST explicitly in \mathbf{x} allows diagnosis of tropical-North Pacific interactions through \mathbf{L}_{NT} and \mathbf{L}_{TN} (Newman et al. 2000; Winkler et al. 2001). Also, since \mathbf{x}

represents annual means, the noise can include variability that, while not predictable over the course of an entire year, may be predictable for a few months.

Defining the state vector solely in terms of SST is perhaps necessary given data limitations for other atmospheric and oceanic circulation variables. Certainly, other variables related to important physical processes such as surface fluxes and oceanic advection are important to SST evolution. The inverse model does, however, *implicitly* include the effects of all other variables linearly related to SST. This is an important distinction from a forward dynamical model in which the evolution of the state vector is governed only by the *explicitly* represented interactions among its components.

The leading 7 EOFs of anomalous Tropical SST and the leading 3 EOFs of anomalous North Pacific SST were retained for the model. The time-varying coefficients of these EOFs, i.e., the principal components (PCs), define a 10-component state vector \mathbf{x} . The retained tropical SST EOFs account for 91% of tropical variance, while the North Pacific SST EOFs capture about 80% of the variance in the central and western North Pacific, though only about 64% of the domain-integrated variance. A lag of $\tau_0=1$ yr was used to determine \mathbf{L} . Constructing a LIM from longer lags and/or more EOFs produces qualitatively similar results for \mathbf{G} , but results in the Nyquist problem for \mathbf{L} discussed in section 2.

Finally, the LIM must be tested on data independent of that used to determine \mathbf{L} . Estimates of \mathbf{L} and of forecast skill were cross-validated as follows. We sub-sampled the data record by removing one decade, computed \mathbf{L} via (3) for the remaining years, and then generated forecasts for the independent years. This procedure was repeated for each

year. All measures of forecast skill in this study are based upon these jack-knifed forecasts.

4 Results

4.1 Forecast skill

Figure 2 shows forecast skill $\rho(\tau)$ for forecast leads of one and two years. Here, forecasts are compared with the complete (that is, untruncated in EOF space) gridded observations. Regions of little skill ($\rho < 0.2$) in the North Pacific coincide with regions where relatively less variance is explained by the leading three EOFs. Additional EOFs in \mathbf{x}_N increase skill to be no worse than about $\rho = 0.3$ in the Northeast Pacific for a one-year forecast, with higher-skill regions essentially unchanged.

For two-year forecasts, highest LIM skill lies primarily outside the ENSO region. However, persistence skill is also high, especially in the far west Pacific and Indian ocean, so that differences between LIM and persistence skill (bottom two panels of Fig. 2) are often small. The exception is the tropical Pacific, where persistence skill is negative due to the pronounced interannual cycle of ENSO. Additional EOFs greatly reduce, but do not eliminate, the large negative difference in the Northeast Pacific in the bottom panels.

Examining skill by EOF (Fig. 3) shows good PDO and ENSO one-year forecast skill. In particular, inspection of the forecasts (not shown) finds that all notable transitions into positive and negative ENSO states are captured, as is possible for multivariate, but not for univariate, red noise. PDO one-year skill here ($\rho = 0.64$) may be closer to a realistic

estimate of skill than PDO skill in NCA ($\rho = 0.74$) since ENSO skill is no longer perfect. For both the PDO and ENSO, however, skill drops significantly for two-year forecasts.

4.2 Power spectra

As discussed in section 2.2, if (2) is a good model of \mathbf{x} , the LIM should reproduce the entire power spectra of \mathbf{x} . As a test, (2) is integrated forward for 100000 yr, using the method described in Penland and Matrosova (1994). The noise is generated by $\xi = \sum_j \mathbf{q}_j \eta_j r_j(t)$, where \mathbf{q}_j and $(\eta_j)^2$ are the eigenvectors and eigenvalues, respectively, of \mathbf{Q} , and $r_j(t)$ are independent Gaussian white noises with unit variance. One eigenvalue of \mathbf{Q} is negative with small magnitude, representing insufficient sampling of the most strongly damped eigenmode of \mathbf{L} (below). Reducing the projection of the noise upon this eigenmode by one-third results in a positive definite \mathbf{Q} . Note that any truncation of \mathbf{Q} means that the LIM will not exactly replicate \mathbf{C}_0 .

The resulting “data” is separated into 1000 100-yr time series. The observed spectra and the ensemble mean of the model spectra, determined using the Thomson multitaper method (Thomson 1982; Mann and Lees 1996), for the three leading PCs of both Tropical and North Pacific SST are shown in Figs. 4 and 5. Also, with 1000 realizations, the 95% confidence interval, shown with gray shading, can be determined in a Monte Carlo sense.

The LIM reproduces the main features of the observed power spectra for all the PCs (including the remaining Tropical SST PCs not shown) on all timescales. Obviously, the mean LIM spectra are much smoother than observed, due to the relatively few degrees of freedom in the truncated EOF space. On the other hand, the irregularity of the observed spectra may simply be due to sampling, since no statistically significant peaks exist in the

observed spectra *relative to multivariate red noise*. The confidence intervals reflect substantial variation in the spectra of each 100-yr segment from the model run. Each segment can have pronounced peaks not always coincident with the observed peaks, as exhibited by the spectra of two different 100-yr segments also in Figs. 4 and 5. That is, this multivariate linear system implies that, if good SST data for the last few hundred years were available, we would find interannual and interdecadal spectral peaks for past centuries to be centered at somewhat different frequencies and have different amplitudes and/or widths compared to the twentieth century, without any change in the underlying dynamics on interannual and interdecadal timescales. This point has been emphasized for ENSO variability by Penland and Matrosova (1994), who constructed a LIM of three-month running mean tropical SST that reproduced not only the spectra but also the case-to-case evolution of both warm and cold ENSO events.

Additionally, while for the entire model run the correlation of PDO with ENSO is 0.63 (observed $r=0.69$), the correlation varies between 0.37 and 0.82 (95% confidence interval: 0.48-0.75) when computed from individual 100 year segments. For 5-year running means of the model output (that is, filtering to remove interannual variability) the range is even greater: the correlation for the full run is 0.64 (observations is 0.73) but for 100-yr segments the 95% confidence interval is 0.33-0.85. Similarly, while the observed PDO-ENSO correlation varies from 0.77 to 0.67 for the two halves of the data record, correlation within individual 50-year segments of the model runs varies between 0.26 and 0.87 (95% confidence interval: 0.42-0.79). Again, since \mathbf{L} is constant, this variation is entirely due to noise in this multivariate system, suggesting that large changes in correlations between climate indices also do not necessarily reflect any change in the

underlying dynamics, even on decadal timescales. Obviously, changes in dynamics on millennial timescales (e.g., Tudhope et al. 2001) are not ruled out here.

4.3 *Eigenanalysis of the linear dynamical operator*

To understand departures of both observed and LIM spectra from univariate red noise, we next perform an eigenanalysis of \mathbf{L} . First, a caveat. It is always tempting to separate variability into a set of modes. However, variability results from the sum of contributions of the *complete* set of eigenmodes of \mathbf{L} ,

$$9) \quad \mathbf{x} = \sum_j \mathbf{u}_j \alpha_j(t),$$

where $\alpha_j(t)$ is the projection time series for the j th eigenmode. Unlike techniques that order modes by decreasing amount of variance (or covariance or correlation) explained, the least damped eigenmode is not required to explain the most variance. In fact, eigenmodes are generally not orthogonal (since \mathbf{L} is generally not self-adjoint) and thus variance cannot be partitioned into individual modes. Eigenmodes are useful to the extent they provide insight into the dynamics represented by \mathbf{L} and hence into the predictability.

The eigenvalues and e-folding times (eft) of \mathbf{L} are listed in Table 1, and leading eigenmodes (also sometimes called principal oscillation patterns, or POPs; Hasselmann 1988; Penland 1989) are shown in Fig. 6. Eigenmode time series in Fig. 7 are determined by projecting the data onto the corresponding (biorthogonal) adjoint vectors \mathbf{v}_j ; that is, \mathbf{v}_j are the eigenmodes of the adjoint operator \mathbf{L}^\dagger defined under the L2 norm, so that $\mathbf{u}_i \bullet \mathbf{v}_j = \delta_{ij}$ and thus $\alpha_j(t) = \mathbf{x} \mathbf{v}_j^*$ (e.g., Strang 1988; Farrell 1988). The two leading propagating eigenmodes ($\sigma_i \neq 0$) are reminiscent of a so-called “decadal ENSO” pattern

(Figs. 6a and b; \mathbf{u}_3) and an “interannual ENSO” pattern (Figs. 6c and d; \mathbf{u}_4). Both of these eigenmodes are needed to reproduce ENSO: α_4 (α_3) is correlated with the leading tropical PC at 0.69 (0.43) (see also Penland and Sardeshmukh 1995). Phase propagation is such that the tropical SST anomaly leads the North Pacific anomaly, by about two years in the decadal ENSO (not shown) and by about one year in the interannual ENSO. As is typical of studies filtering Pacific SSTs into interannual and interdecadal bands (e.g., Zhang et al. 1997), the tropical SST portion of \mathbf{u}_3 has broader latitudinal extent than for \mathbf{u}_4 . The North Pacific anomaly is also relatively stronger, consistent with the “reddened ENSO” null hypothesis (NCA). In addition, \mathbf{u}_3 has maximum tropical amplitude nearer to the dateline than \mathbf{u}_4 , which could reflect not only greater decadal variability (e.g., Hazeleger et al 2005) but also greater extratropical sensitivity to SST anomalies in this location (Alexander et al. 2002; Barsugli and Sardeshmukh 2002). One might be tempted to relate the cosine and sine phases of \mathbf{u}_3 . However, the eft is so short that in the presence of noise not even a quarter cycle can likely exist; consequently, neither propagating eigenmode oscillates with a well-defined period (Fig. 7).

The two leading eigenmodes (Figs. 6e and f) are stationary and have considerably longer efts than any other eigenmode. Unsurprisingly, these eigenmodes also display the greatest persistence. [In contrast, the amplitude of the most damped eigenmode, also in Fig. 7, changes sign almost yearly.] The leading eigenmode, \mathbf{u}_1 , looks very similar to the 1900-2002 trend pattern (not shown), which also shows pronounced warming along the western and northern boundaries of the Pacific Ocean and in the Indian Ocean, with little amplitude in the ENSO and PDO regions. In fact, $\alpha_1(t)$ is highly correlated ($r = 0.86$) with July-June global mean temperature determined from the monthly NASA GISS

Surface Temperature Analysis (GISTEMP) dataset (<http://data.giss.nasa.gov/gistemp/>; Hansen et al 1996, 1999, 2001; Reynolds et al 2002; red line in Fig. 7); note that amplitude of both time series decreases from the mid 1940's to the mid 1960's. The tropical portion of \mathbf{u}_1 is also very similar to the least damped eigenmode from a LIM constructed of three-month running mean Tropical SSTs during 1950-2002. Penland and Matrosova (2006) suggest this eigenmode may represent tropical variability separate from canonical ENSO evolution that nevertheless impacts ENSO predictability, and found that its associated time series peaked in the mid-1980's. However, including the North Pacific results in a time series that continues to increase beyond this time (Fig. 7). The observed \mathbf{u}_1 trend is greater than almost 95% of the \mathbf{u}_1 trends in all 102-yr segments of the LIM model.

The second eigenmode, \mathbf{u}_2 , has strong amplitude in the North Pacific, with the maximum located west of the PDO maximum. The tropical amplitude is relatively weaker, although there is an equatorial maximum at the dateline, off-equatorial maxima in the eastern Pacific, and again a relatively large Indian Ocean anomaly. Similar features have been found by previous decadal variability studies. For example, \mathbf{u}_2 resembles the “global signal” found by Livezey and Smith (1999) in a rotated canonical correlation analysis of SST and United States surface temperatures for the 1950-92 period. Livezey and Smith suggested that this pattern reflected a trend possibly related to global warming, and as it is quite similar to the post-1950 trend pattern, it might be expected to dominate their analysis. The tropical portion of \mathbf{u}_2 also resembles the pattern identified by Deser et al. (2004) as related to an interdecadal signal, or “epoch difference,” in the Aleutian low, although their North Pacific anomaly is further east than in \mathbf{u}_2 , perhaps because their

epoch difference pattern also appears to include a contribution from \mathbf{u}_3 . Their analysis of 1900-1998 data suggested that their pattern did not represent a long-term trend but rather had undergone a few changes of sign in the twentieth century; a successor study (D'Arrigo et al. 2006) found other possible sign reversals of the pattern before 1900. Almost half of the 102-yr segments of the model run have larger \mathbf{u}_2 trends than observed.

The above results are qualitatively similar for different EOF truncations and different dataset periods. There are some quantitative changes in the eigenvalues, however. For example, removing different decades from the dataset (as in the cross-validation) makes the eft for the leading (second) eigenmode vary between 12 and 18 (4 and 7) years. Likewise, periods of propagating eigenmodes vary, between about 20 and 40 years for \mathbf{u}_3 and between about 4.5 and 7 years for \mathbf{u}_4 . Using the Kaplan dataset instead produces eigenvalues that also fall in these ranges, although all eigenmodes are more damped than their HadISST counterparts. Common to all cases, however, are two leading stationary eigenmodes plus an overdamped decadal ENSO eigenmode clearly distinct from an interannual ENSO eigenmode, all with the spatial characteristics described above.

Stratifying forecast skill by eigenmode rather than by EOF clarifies the source of predictability. Results for forecast leads of one and two years are shown in Fig. 8, compared to predicted skill determined from the LIM using (6). Now apparent random variation of skill by PC (Fig. 3) is replaced by a strong relationship between skill and eft. For forecast leads beyond one year, useful skill resides primarily in the two leading eigenmodes, also clearly reflected in the forecast skill maps (Fig. 2). In fact, skill for \mathbf{u}_2 is above 0.5 for forecast leads up to 6 years. Note that little long-range skill is associated with \mathbf{u}_3 , despite its long period, because its eft is so short.

In eigenmode space, (2) becomes a set of uncoupled univariate equations,

$$10) \frac{d\alpha_j}{dt} = \lambda_j \alpha_j + \hat{\xi}_j,$$

where $\hat{\xi}_j$ is white noise in eigenmode space. Another test of the LIM, and of the eigenmodes themselves, is to determine whether $\hat{\xi}_j$ represents white noise, and consequently whether each time series $\alpha_j(t)$ is univariate red noise. Consistent with the assumption of white noise we find that $\hat{\xi}_j$, calculated as a residual from (10), is normally distributed and almost uncorrelated from year to year.

4.4 Reconstructing the PDO as a sum of univariate red noises

No single eigenmode can be identified as “the” PDO. That is, no individual time series $\alpha_j(t)$ correlates with the PDO at a value higher than 0.47. Yet the LIM reproduces the entire PDO spectrum, suggesting that the PDO represents not a single mode but rather a superposition of different modes acting on different spatial and temporal scales. This is illustrated in Fig. 9 by comparing the observed PDO time series $P(t)$ to a reconstruction from the sum of just three eigenmodes, $\tilde{P}(t) = \mathbf{u}_2\alpha_2(t) + \mathbf{u}_3\alpha_3(t) + \mathbf{u}_4\alpha_4(t)$. The correlation of \tilde{P} and P is 0.8; the difference $d = P - \tilde{P}$ is mostly noise (the decorrelation timescale of d is less than one year) that projects on the most strongly damped eigenmodes. Interestingly, including \mathbf{u}_2 , which has large amplitude in the PDO region, is important even though the correlation of α_2 and the PDO is 0.2, because without it \tilde{P} is correlated with P at only 0.65.

Fig. 9 also notes years commonly associated with “regime shifts” in the PDO (e.g., Hare and Mantua 2000; Deser et al. 2004). \tilde{P} clearly reproduces these shifts, but here they represent not nonlinear state changes but rather random changes due to the summation of these univariate red noises. Also, these shifts arise from neither constructive interference nor phase-locking of multidecadal oscillations of differing periods (e.g., Minobe 1999). Since the eigenmodes that contribute to the PDO are nonorthogonal, a white noise “kick” can perturb all three modes to some degree. On the other hand, the regime shifts do not seem to correspond to consistent changes of the three eigenmodes. For example, while the shift in the early 1940’s occurs as \mathbf{u}_2 begins a long period of negative values (after a period of weakly positive to neutral values), the mid 1970’s shift occurs about a decade after \mathbf{u}_2 changed sign. Some authors have also suggested a shift occurred in 1998, but as of mid-2002 the PDO has had mostly positive values (not shown). This possibly transitory excursion of negative PDO values is consistent with the strong negative excursion of \mathbf{u}_3 , which due to its very short eft is unlikely to be short-lived.

5 Impact of Tropical-North Pacific coupling

As noted in section 3, (8) allows diagnosis of the impact of tropical-North Pacific coupling upon SST variability. This is done by first repeating the model run of section 4.2, executing additional 100000 yr runs in which either (1) the Tropics and North Pacific are uncoupled ($\mathbf{L}_{TN} = \mathbf{L}_{NT} = 0$), and noise in the Tropics and North Pacific is uncorrelated ($\langle \xi_N \xi_T^T \rangle = 0$) (“fully uncoupled”); (2) the Tropics and North Pacific are uncoupled ($\mathbf{L}_{TN} = \mathbf{L}_{NT} = 0$), but the original correlated noise eigenmodes are used; that is, noise fluctuates with coherent tropical-North Pacific patterns (“partially uncoupled”);

(3) the Tropics do not force the North Pacific ($\mathbf{L}_{TN} = 0$) and $\langle \boldsymbol{\xi}_N \boldsymbol{\xi}_T^T \rangle = 0$); or (4) the North Pacific does not force the Tropics ($\mathbf{L}_{NT} = 0$ and $\langle \boldsymbol{\xi}_N \boldsymbol{\xi}_T^T \rangle = 0$). Runs (3) and (4) are repeated with the tropical-North Pacific correlated noise included. The fully uncoupled model (green lines in Figs. 4 and 5) results in two independent dynamical systems,

$$11) \frac{d\mathbf{x}_N}{dt} = \mathbf{L}_{NN}\mathbf{x}_N + \boldsymbol{\xi}_N$$

and

$$12) \frac{d\mathbf{x}_T}{dt} = \mathbf{L}_{TT}\mathbf{x}_T + \boldsymbol{\xi}_T.$$

Note that \mathbf{L}_{NN} is different than the linear operator (say, $\hat{\mathbf{L}}_{NN}$) that would be obtained from the LIM of just \mathbf{x}_N alone, since the latter would involve actual evolution of North Pacific SST, which includes tropical forcing. That is, we are trying to *remove* the effects of \mathbf{x}_N upon \mathbf{x}_T and vice versa, so that (11) represents only “internal” North Pacific dynamics and (12) represents only “internal” tropical dynamics. As an important caveat, “coupling” here refers to the relationship of \mathbf{x}_N with \mathbf{x}_T , without differentiating either which parts of the state vectors are most important or whether the connections are through the atmosphere and/or through the ocean.

PDO-ENSO correlations for each run, for both annual means and five-year running means, are compared with correlations from the full LIM and from observations in Fig. 10a. Coherence between the PDO and ENSO (Fig. 10b) shows no interannual PDO-ENSO relationship when the Tropics do not force the North Pacific. Conversely, there is

no predictable effect of the North Pacific upon the Tropics on interannual timescales, although there is an unpredictable effect that occurs when noises in the Tropics and North Pacific are spatially correlated, a result consistent with seasonal footprinting (Vimont et al. 2001, 2003; Seager et al. 2004). On decadal timescales, the PDO-ENSO relationship is about equally dependent upon tropical and North Pacific forcing.

How coupling affects \mathbf{L} can be understood through eigenanalysis of the uncoupled dynamical system (11) and (12). Eigenanalysis of \mathbf{L}_{NN} results in a pair of propagating eigenmodes with an 18.8 yr period and 3.9 yr eft, and one strongly damped (0.5 yr eft) stationary eigenmode. The propagating eigenmode is consistent with behavior found in many models of North Pacific variability: an initial SST response to anomalous surface forcing in the central North Pacific (Fig. 11a) followed by a remote response in the KOE region (Fig. 11b) due to westward propagating (bottom panels of Fig. 11) oceanic Rossby waves with subsurface temperature anomalies brought to the surface in the KOE by mixing and/or gyre adjustment (e.g., Qiu 2000; Xie et al. 2000; Seager et al. 2001; Schneider et al. 2002). The eft is only long enough to follow a Rossby wave to the KOE, consistent with earlier studies (Seager et al. 2001; Schneider and Miller 2001) suggesting that knowledge of wind stress forcing over the North Pacific could result in predictability of a few years in the western North Pacific.

Furthermore, the North Pacific power spectra resulting from the fully uncoupled run (Fig. 5) show much more North Pacific decadal variability than for either the full LIM or observations, with the peak centered slightly less than the uncoupled eigenmode period because of the shorter eft. Thus, while \mathbf{L}_{NN} is consistent with previous theoretical and simple modeling studies of the North Pacific, the full dynamical operator is needed to

reproduce observations; that is, consideration of internal North Pacific dynamics without tropical interactions appears insufficient to understand North Pacific variability.

While the leading tropical PC is only weakly affected by the North Pacific, coupling enhances decadal variability of the remaining tropical PCs (Fig. 4). This is consistent with the eigenmodes of \mathbf{L}_{TT} (not shown): the leading propagating eigenmode looks very similar to the tropical portion of \mathbf{u}_4 (Figs. 6cd) with only a minor increase in period and eft, and the other \mathbf{L}_{TT} eigenmodes also have counterparts in the eigenmodes of the full operator \mathbf{L} but are relatively more damped.

The leading coupled eigenmode \mathbf{u}_1 has no clear counterpart in the uncoupled eigenmodes, a considerably longer eft than any eigenmode of either \mathbf{L}_{TT} or \mathbf{L}_{NN} , and a tropical pattern that looks nothing like any eigenmode of \mathbf{L}_{TT} . Similarly, while tropical and North Pacific counterparts to \mathbf{u}_2 exist in the uncoupled eigenmodes, their efts are shorter, especially for the North Pacific. Furthermore, maxima of multidecadal variance for both the Tropics (PC 2) and North Pacific (PC 2 and 3) do not exist for the uncoupled system. This suggests that these eigenmodes and spectral peaks reflect a fundamentally coupled process.

6 Comparison to coupled GCMs

How well the dynamical system of observed Pacific SST described in this paper is replicated in coupled atmosphere-ocean GCMs is investigated for output from the Coupled Model Intercomparison Project (CMIP) for the current IPCC Fourth Assessment Report (AR4). The models, along with the lengths of the control runs used, are listed in Table 2; further details are available at <http://www->

pcmdi.llnl.gov/projects/cmip/index.php. As with the HadISST data, the GCM datasets were averaged, and/or interpolated where necessary, to the same grid and July-June annual means. Anomalies were then determined by removing the model climatology. For consistent comparison, and because it is the real system these sophisticated models are trying to simulate, the model data were projected onto the observed EOFs to produce PC time series in each model. Earlier analyses of CMIP model data (AchtuaRao and Sperber 2002, 2006) that tended to claim somewhat better results for ENSO simulation were focused on an index of NINO3, a region in which model simulations are perhaps least erroneous (not shown).

It is occasionally suggested that GCMs may appear different than the observed system because they represent different realizations of the climate state, not necessarily different physics. If we interpret the LIM confidence intervals as showing the possible range of realizations, however, then the spectra of all of the models (not shown) are statistically significantly different from the observed system. Differences between GCM and observed variability are also readily apparent by comparing the variance of Tropical (Fig. 12) and North Pacific (Fig. 13) PCs, for both annual and five-year running means. Many of the models have an ENSO spectral peak whose period is too short, a well-known coupled GCM problem; not surprisingly, these models also have relatively too much variance on interannual timescales. In fact, virtually all the GCMs have tropical decadal variability that is less than observed. On the other hand, there is no apparent systematic error in the variance of the North Pacific PCs; most of the GCMs lie outside the LIM confidence intervals on annual timescales but are within the intervals on decadal

timescales. Perhaps most important, all the GCMs consistently underestimate the PDO-ENSO correlation on both annual and decadal timescales, as is shown in Fig. 14.

The leading eigenmodes likewise are inadequately simulated. As an example, the GCM data are projected onto these eigenmodes. Decorrelation timescales, the time the autocorrelation function has decreased to $1/e$, are then determined for the resulting time series; note that for the propagating modes, the decorrelation includes the effect of propagation as well. These timescales are compared with the observed decorrelation timescales in Fig. 15. The leading eigenmodes show much less persistence in the GCMs than is observed. This is true even if the observed time series are detrended, which shortens the decorrelation timescale of u_1 to about 3 yrs while leaving the other decorrelation timescales unchanged.

This combination of underestimating both tropical decadal variability and ENSO-PDO correlation yet having more reasonable estimates of North Pacific decadal variability, along with low persistence of the leading eigenmodes, suggests that North Pacific SSTs in these GCMs may be too independent of the Tropics.

7 Concluding Remarks

A multivariate red noise model, empirically constructed from a one-year lag, can explain the observed power spectra of annual mean Tropical and North Pacific SST on both interannual and interdecadal timescales. Spectral peaks on decadal timescales that may represent slow physical oceanic processes also correspond to strongly damped propagating eigenmodes, so that predictability on these timescales is low (Scott 2003 makes a similar point). Forcing of the North Pacific by the Tropics, and also forcing of

the Tropics by the North Pacific, is a critical element of Pacific decadal variability and predictability that appears poorly represented in coupled GCMs. The range of these GCM simulations appears outside what might be expected from a series of “real world” realizations, despite the fact that substantial variations in both the power spectra of, and the correlations between, the Tropics and North Pacific are possible even if the dynamics of annual-mean SST are fixed and multilinear. Thus, previous studies employing coupled GCMs likely underestimated the tropical contribution to North Pacific decadal variability and predictability.

Virtually all long-range LIM skill comes from two stationary eigenmodes that have the longest e-folding times. Anomaly correlation skill of both eigenmodes is greater than 0.5 for up to six years. The timeseries of the leading eigenmode has a 100-yr trend that is unlikely, but not impossible, to have occurred by chance in the multivariate linear system. The second eigenmode has a pattern somewhat similar to the multidecadal signal found by Deser et al. (2004) and D’Arrigo et al. (2006) and might represent natural decadal variability. Note, however, that this eigenmode does not *propagate* with a multidecadal period, but instead has a sufficiently long eft that it varies on a decadal timescale². Both modes appear to have persistence and thus predictability significantly enhanced by Tropical-North Pacific coupling, and are poorly simulated by the coupled GCM control runs examined here. Whether one or both eigenmodes represent anthropogenic forcing (as suggested by Livezey and Smith (1999)), other external radiative forcing, natural decadal variability that these GCMs cannot capture, or some combination of the three, remains undetermined by our analysis. Certainly, the time series of the leading

² The ideal name for this mode would then of course be the Pacific Multidecadal Fluctuation (PMF).

eigenmode has a strong correspondence to the global mean temperature trend often associated with anthropogenic effects. Of course, if the two least damped eigenmodes include externally forced variability, they should not be fully simulated by the IPCC control runs; definitive assessment awaits repetition of this analysis upon coupled GCMs forced with historical changes in radiative forcing. These eigenmodes might also represent nonstationarity artificially introduced by the SST reconstruction technique applied to differing amounts and quality of input data, but it is encouraging that the HadISST bias correction has a different spatial pattern than either eigenmode (Folland and Parker 1995), that in the Tropics the leading eigenmode has a different pattern than that of observation locations (Penland and Matrosova 2006), and that both eigenmodes also result from LIMs of post-1950 SST datasets, either annual means (not shown) or three-month running means (Penland and Matrosova 2006).

Much of the interest in the PDO has come from its apparent relationship with regime shifts throughout the climate system and possibly in the marine ecosystem as well. There has been related interest in whether the PDO might represent a “long-memory” process or $1/f$ noise, with much more regime-like behavior than exists in univariate red noise (Percival et al. 2001; Rudnick and Davis 2003; Overland et al. 2006; see also Fraedrich et al. 2004). Such behavior might be characteristic, for example, of the slow manifold of a nonlinear dynamical system. Also, nonlinear models have been proposed to account for the decadal variability of ENSO (e.g., Tziperman et al. 1995; Timmermann and Jin 2002; Karspeck et al 2004) and it might be expected that, at a minimum, regime shifts in the Tropics would produce regime shifts in the North Pacific (Seager et al 2004). However, it is well known that long-memory behavior exists in processes that are the sum of

independent red noises (Beran 1994). Also, a multivariate linear system representing advection and diffusion, driven by Gaussian white noise, can produce $1/f$ noise (Milotti 1995). Our results suggest that, on the annual time scale, the PDO represents not a single phenomenon but rather the sum of several different basin-scale processes (see also Schneider and Cornuelle 2005), each of which represent different spatial patterns whose temporal evolution can be separately modeled as red noise with differing autocorrelation timescales. Then, apparent PDO “regime shifts” are best understood not as sudden, yet potentially predictable, nonlinear changes between relatively stable climate states, but rather as *random occurrences in a multivariate linear system driven by noise*. Importantly, in this view regime shifts are not predictable beyond the timescale of the most rapidly decorrelating red noise, less than two years. In addition, once a regime shift has occurred, the expected duration of the regime may be predicted, depending upon the relative contributions of different eigenmodes. Based on this model, it appears unlikely that 1998 marked the beginning of a long period of negative PDO values.

This dynamical model of annual-mean SST may constrain possible physical models of coupled atmosphere-ocean Pacific decadal variability. For example, predictable effects of the North Pacific upon the Tropics are associated with only stationary modes, as opposed to propagating modes where, say, North Pacific SST leads tropical SST. This result seems more consistent with atmospheric rather than oceanic teleconnections between the North Pacific and the Tropics, since it suggests a rapid (less than a year) connection between the two regions. Also, a theory that produces fairly regular cycling of anomalies on decadal timescales could be inconsistent with the short life of \mathbf{u}_3 . To the extent that

coupling appears important on decadal timescales, a physical model that considers just the North Pacific in isolation, or just the Tropics, will probably not explain observed variability. As a caveat, note that the LIM does not imply that realistic physical models must be *actually* linear, but rather be *effectively* linear; that is, with little nonlinear predictability on annual timescales. Ultimately, in the LIM framework further questions about important physical processes, as well as gauging the impact of predictable nonlinearities on seasonal timescales, will require explicitly including both atmospheric and subsurface ocean data in the state vector, using shorter time averaging and including seasonality, issues which are being considered in our current research. Surface heat fluxes may include state-dependent, or multiplicative, noise (Sura et al. 2005; 2006), which could also affect our results.

Finally, decadal SST predictability does not necessarily equal decadal atmospheric predictability. Previous coupled GCM studies found some decadal predictability over ocean but also considerably lower predictability over land (e.g., Grotzner et al 1999; Pohlmann et al. 2004). Similarly, the fraction of variance on decadal timescales is much higher for SST than for surface pressure over the North Pacific (NCA). In fact, decadal signals in Pacific SST may be best used to forecast climate integrators, variables such as soil moisture and snowpack that tend to integrate anomalous climate forcing, which may have a stronger relationship to North Pacific SST than instantaneous atmospheric variables such as surface temperature (NCA). Alternatively, since operational seasonal North American temperature forecasts have some skill using the previous ten year mean (Huang et al. 1994), small additional skill may be gained by instead using a bivariate predictor based on the leading two eigenmodes of \mathbf{L} .

Acknowledgements

Conversations with many coworkers at the lab formerly known as CDC greatly advanced the development of this study, particularly Mike Alexander, Gil Compo, Cécile Penland, Prashant Sardeshmukh, Amy Solomon, and Cathy Smith. Comments by Rob Scott and an anonymous reviewer improved the manuscript. Jamie Scott assisted with obtaining the IPCC model dataset. We acknowledge the international modeling groups for providing their data for analysis and the Program for Climate Model Diagnosis and Intercomparison (PCMDI) for collecting and archiving the model data. The IPCC Data Archive at Lawrence Livermore National Laboratory is supported by the Office of Science, U.S. Department of Energy. This work was partially supported by a grant from NOAA CLIVAR/Pacific.

8 References

- AchutaRao, K., and K. R. Sperber, 2002: Simulation of the El Niño Southern Oscillation: Results from the Coupled Model Intercomparison Project. *Climate Dyn.*, **19**, 191-209.
- AchutaRao, K. and K. R. Sperber, 2006: ENSO simulation in coupled ocean-atmosphere models: Are the current models better? *Climate Dyn.*, 10.1007/s00382-006-0119-7.
- Alexander, M. A., C. Deser, and M. S. Timlin, 1999: The re-emergence of SST anomalies in the North Pacific Ocean. *J. Climate*, **12**, 2419–2431.
- Alexander, M. A., I. Bladé, M. Newman, J. R. Lanzante, N.-C. Lau, and J. D. Scott, 2002: The atmospheric bridge: The influence of ENSO teleconnections on air–sea interaction over the global oceans. *J. Climate*, **15**, 2205–2231.
- An, S.-I., and B. Wang, 2005: The forced and intrinsic low-frequency modes in the North Pacific. *J. Climate*, **18**, 876-885.
- Barnett, T. P., D. W. Pierce, M. Latif, D. Dommenget, and R. Saravanan, 1999: Interdecadal interactions between the Tropics and midlatitudes in the Pacific basin. *Geophys. Res. Lett.*, **26**, 615-618.
- Barsugli, J. J., and D. S. Battisti, 1998: The basic effects of atmosphere-ocean coupling on midlatitude variability. *J. Atmos. Sci.*, **55**, 477-493.

- Barsugli, J. J., and P. D. Sardeshmukh, 2002: Global atmospheric sensitivity to tropical SST anomalies throughout the Indo-Pacific Basin. *J. Climate*, **15**, 3427-3442.
- Benson, A. J., and A. W. Trites, 2002: Ecological effects of regime shifts in the Bering Sea and eastern North Pacific Ocean. *Fish and Fisheries*, **3**, 95-113.
- Beran, J., 1994: *Statistics for long-memory processes*. Chapman and Hall, New York, 315 pp.
- Biondi, F., A. Gershunov, and D. R. Cayan, 2001: North Pacific decadal climate variability since 1661. *J. Climate*, **14**, 5–10.
- Bond, N. A., J. E. Overland, M. Spillane, P. Stabeno, 2003: Recent shifts in the state of the North Pacific. *Geophys. Res. Lett.*, **30**, doi:10.1029/2003GL018597.
- Chang, P., R. Saravanan, T. DelSole, and F. Wang, 2004: Predictability of linear coupled systems. Part I: Theoretical analyses. *J. Climate*, **17**, 1474-1486,
- D'Arrigo, R., R. Villalba, and G. Wiles, 2001: Tree-ring estimates of Pacific decadal climate variability. *Climate Dyn.*, **18**, 219–224.
- DelSole, T., and A. Y. Hou, 1999: Empirical stochastic models for the dominant climate statistics of a general circulation model. *J. Atmos. Sci.*, **56**, 3436—3456.
- Deser, C., and M. L. Blackmon, 1995: On the relationship between tropical and North Pacific sea surface temperatures. *J. Climate*, **8**, 1677-1680.

- Deser, C., A. S. Phillips, and J. W. Hurrell, 2004: Pacific interdecadal climate variability: Linkages between the Tropics and the North Pacific during Boreal winter since 1900. *J. Climate*, **17**, 3109-3124.
- Evans, M. N., M. A. Cane, D. P. Schrag, A. Kaplan, B. K. Linsley, R. Villalba, and G. M. Wellington, 2001: Support for tropically-driven Pacific decadal variability based on paleoproxy evidence. *Geophys. Res. Lett.*, **28**, 3689–3692.
- Farrell, B., 1988: Optimal excitation of neutral Rossby waves. *J. Atmos. Sci.*, **45**, 163-172.
- Folland, C. K., and D. E. Parker, 1995: Correction of instrumental biases in historical sea surface temperature data. *Q. J. R. Meteor. Soc.*, **121**, 319-367.
- Fraedrich, K., U. Luksch, and R. Blender, 2004: $1/f$ model for long-time memory of the ocean surface temperature. *Phys. Rev. E*, **70**, 037301.
- Frankignoul, C., and K. Hasselmann, 1977: Stochastic climate models. Part II: Application to sea-surface temperature anomalies and thermocline variability. *Tellus*, **29**, 284–305.
- Frankignoul, C., P. Müller, and E. Zorita, 1997: A simple model of the decadal response of the ocean to stochastic wind forcing. *J. Phys. Oceanogr.*, **27**, 1533-1546.
- Grotzner, A., M. Latif, A. Timmermann, and R. Voss, 1999: Interannual to decadal predictability in a coupled ocean-atmosphere general circulation model. *J. Climate*, **12**, 2607-2624.

- Gu, D., and S. G. H. Philander, 1997: Interdecadal climate fluctuations that depend on exchange between the tropics and extratropics. *Science*, **275**, 805-807.
- Hansen, J., R. Ruedy, M. Sato and R. Reynolds, 1996: Global surface air temperature in 1995: Return to pre-Pinatubo level. *Geophys. Res. Lett.*, **23**, 1665-1668.
- Hansen, J., R. Ruedy, J. Glascoe, and M. Sato, 1999: GISS analysis of surface temperature change. *J. Geophys. Res.*, **104**, 30997-31022.
- Hansen, J., R. Ruedy, M. Sato, M. Imhoff, W. Lawrence, D. Easterling, T. Peterson, and T. Karl, 2001: A closer look at United States and global surface temperature change. *J. Geophys. Res.*, **106**, 23947-23963
- Hasselmann, K., 1976: Stochastic climate models. Part I. Theory. *Tellus*, **28**, 474-485.
- Hasselmann, K., 1988: PIPs and POPs: the reduction of complex dynamical systems using principal interaction and oscillation patterns. *J. Geophys. Res.*, **93**, 11 015-11 021.
- Hazeleger, W., C. Severijns, R. Seager, F. Molteni, 2005: Tropical Pacific-driven decadal energy transport variability. *J. Climate*, **18**, 2037-2051.
- Huang, J., H. M. van den Dool, and A. G. Barnston, 1994: Long-lead seasonal temperature prediction using optimal climate normals. *J. Climate*, **9**, 809-817.
- Jin, F-F., 1997: A theory of interdecadal climate variability of the North Pacific ocean-atmosphere system. *J. Climate*, **10**, 1821-1835.

- Johnson, S. D., D. S. Battisti, and E. S. Sarachik, 2000: Empirically derived Markov models and prediction of Tropical Pacific sea surface temperature anomalies. *J. Climate*, **13**, 3-17.
- Kaplan, A., M. Cane, Y. Kushnir, A. Clement, M. Blumenthal, and B. Rajagopalan, 1998: Analyses of global sea surface temperature 1856-1991. *J. Geophys. Res.*, **103**, 18,567-18,589.
- Livezey, R. E., and T. M. Smith, 1999: Covariability of aspects of North American climate with global sea surface temperatures on interannual to interdecadal timescales. *J. Climate*, **12**, 289-302.
- Mann, M.E. and Lees, J.M., 1996: Robust estimation of background noise and signal detection in climatic time series. *Clim. Change.*, **33**, 409-445.
- Miller, A. J., F. Chai, S. Chiba, J. R. Moisan, and D. J., Neilson, 2004: Decadal-scale climate and ecosystem interactions in the North Pacific ocean. *J. Oceanogr.*, **60**, 163-188.
- Milotti, E., Linear processes that produce $1/f$ or flicker noise. *Phys. Rev. E.*, **51**, 3087-3103.
- Minobe, S., 1999: Resonance in bidecadal and pentadecadal climate oscillations over the North Pacific: Role in climatic regime shifts. *Geophys. Res. Lett.*, **26**, 855-858.
- Nakamura, H., G. Lin, and T. Yamagata, 1997: Decadal climate variability in the North Pacific in recent decades. *Bull. Amer. Meteor. Soc.*, **78**, 2215-2226.

- Newman, M., M. A. Alexander, C. R. Winkler, J. D. Scott, and J. J. Barsugli, 2000: A linear diagnosis of the coupled extratropical ocean atmosphere system in the GFDL GCM. *Atmospheric Sci. Lett.*, **1**, 1-12.
- Newman, M., P. D. Sardeshmukh, C. R. Winkler, and J. S. Whitaker, 2003a: A study of subseasonal predictability. *Mon. Wea. Rev.*, **131**, 1715-1732.
- Newman, M., G. P. Compo, and M. A. Alexander, 2003b: ENSO-forced variability of the Pacific Decadal Oscillation. *J. Climate*, **16**, 3853-3857.
- Overland, J. E., D. B. Percival, and H. O. Mofjeld, 2006: Regime shifts and red noise in the North Pacific. *Deep-Sea Research I*, **53**, 582-588.
- Papanicolaou, G. and W. Kohler, 1974: Asymptotic theory of mixing stochastic ordinary differential equations. *Commun. Pure Appl. Math.*, **27**, 641-668.
- Penland, C., 1989: Random forcing and forecasting using principal oscillation pattern analysis. *Mon. Wea. Rev.*, **117**, 2165—2185.
- Penland, C., 1996: A stochastic model of IndoPacific sea surface temperature anomalies. *Physica D*, **98**, 534--558.
- Penland, C., and M. Ghil, 1993: Forecasting Northern Hemisphere 700-mb geopotential heights using principal oscillation patterns. *Mon. Wea. Rev.*, **121**, 2355—2372.
- Penland, C., and L. Matrosova, 1994: A balance condition for stochastic numerical models with application to the El Niño - Southern Oscillation. *J. Climate*, **7**, 1352-1372.

- Penland, C., and L. Matrosova, 2006: Studies of El Niño and interdecadal variability in Tropical sea surface temperatures using a nonnormal filter. *J. Climate*, in press.
- Penland, C., and P. D. Sardeshmukh, 1995: The optimal growth of tropical sea surface temperature anomalies. *J. Climate*, **8**, 1999—2024.
- Percival, D. B., J. E. Overland, and H. O. Mofjeld, 2001: Interpretation of North Pacific variability as a short- and long-memory process. *J. Climate*, **14**, 4545-4559.
- Pierce, D., 2001: Distinguishing coupled ocean-atmosphere interactions from background noise in the North Pacific. *Prog. Oceanogr.*, **49**, 331-352.
- Pohlmann, H., M. Botzet, M. Latif, A. Roesch, M. Wild, and P. Tschuck, 2004: Estimating decadal predictability of a coupled AOGCM. *J. Climate*, **17**, 4463-4472.
- Qiu, B., 1995: Why is the spreading of the North Pacific intermediate water confined on density surfaces around $\sigma_\theta=28.6$? *J. Phys. Oceanogr.*, **25**, 168-180.
- Qiu, B., 2000: Interannual variability of the Kuroshio extension system and its impact on the wintertime SST field. *J. Phys. Oceanogr.*, **30**, 1486-1502.
- Reynolds, R.W., N.A. Rayner, T.M. Smith, D.C. Stokes, and W. Wang 2002: An improved in situ and satellite SST analysis for climate. *J. Climate*, **15**, 1609-1625.
- Rudnick, D. L., and R. E. Davis, 2003: Red noise and regime shifts. *Deep Sea Research I*, **50**, 691-699.

- Saravanan, R., and J. C. McWilliams, 1998: Advective ocean-atmosphere interaction: An analytical stochastic model with implications for decadal variability. *J. Climate*, **11**, 165-188.
- Sardeshmukh, P.D., G. P. Compo, and C. Penland, 2000: Changes in probability associated with El Niño. *J. Climate*, **13**, 4268-4286.
- Schneider, N., and B. D. Cornuelle, 2005: The forcing of the Pacific Decadal Oscillation. *J. Climate*, **18**, 4355-4373.
- Schneider, N. and A. J. Miller, 2001: Predicting western North Pacific Ocean climate. *J. Climate*, **14**, 3997-4002.
- Schneider, N., A. J. Miller, M. Alexander, and C. Deser, 1999: Subduction of decadal North Pacific temperature anomalies: Observations and dynamics. *J. Phys. Oceanogr.*, **29**, 1056-1070.
- Schneider, N., A. J. Miller, and D. W. Pierce, 2002: Anatomy of North Pacific decadal variability. *J. Climate*, **15**, 586-605.
- Scott, R. B., 2003: Predictability of SST in an idealized, one-dimensional, coupled atmosphere-ocean climate model with stochastic forcing and advection. *J. Climate*, **16**, 323-335.
- Scott, R. B., and B. Qiu, 2003: Predictability of SST in a stochastic climate model and its application to the Kuroshio extension region. *J. Climate*, **16**, 312-322.

- Seager, R., Y. Kushnir, N. H. Naik, M. A. Cane, and J. Miller, 2001: Wind-driven shifts in the latitude of the Kuroshio-Oyashio extension and generation of SST anomalies on decadal timescales. *J. Climate*, **14**, 4249-4265.
- Seager, R., A. R. Karspeck, M.A. Cane, Y. Kushnir, A. Giannini, A. Kaplan, B. Kerman, and J. Velez, 2004: Predicting Pacific decadal variability. In *Earth's Climate: The Ocean-Atmosphere Interaction*, Geophysical Monograph Series 147, 105-120.
- Solomon, A., J. P. McCreary, R. Kleeman, and B. A. Klinger, 2003: Interannual and decadal variability in an intermediate coupled model of the Pacific region. *J. Climate*, **16**, 383-405.
- Strang, G., 1988: *Linear Algebra and its Applications*. Academic Press, 520 pp.
- Sura, P., M. Newman, C. Penland, and P. D. Sardeshmukh, 2005: Multiplicative noise and non-Gaussianity: A paradigm for atmospheric regimes? *J. Atmos. Sci.*, **62**, 1391-1409.
- Sura, P., M. Newman, and M. A. Alexander, 2006: Daily to decadal sea surface temperature variability driven by state-dependent stochastic heat fluxes. *J. Phys. Oceanogr.*, in press.
- Thomson, D.J., 1982: Spectrum estimation and harmonic analysis. *Proc. IEEE*, **70**, 1055-1096.
- Timmermann, A., and F. Jin, 2002: A nonlinear mechanism for decadal El Nino amplitude changes. *Geophys. Res. Lett.*, **29**, 1003-1006.

- Tourre, Y. M., Y. Kushnir, and W. B. White, 1999: Evolution of interdecadal variability in sea level pressure, sea surface temperature, and upper ocean temperature over the Pacific Ocean. *J. Phys. Oceanogr.*, **29**, 1528-1541.
- Trenberth, K., and J. Hurrell, 1994: Decadal atmosphere–ocean variations in the Pacific. *Climate Dyn.*, **9**, 303–319.
- Tudhope, A. W., C. P. Chilcott, M. T. McCulloch, E. R. Cook, J. Chappell, R. M. Ellam, D. W. Lea, J. M. Lough, and G. B. Shimmield, 2001: Variability in the El Nino–Southern Oscillation through a glacial-interglacial cycle. *Science*, **291**, 1511–1517.
- Venzke, S., M. Munnich, and M. Latif, 2000: On the predictability of decadal changes in the North Pacific. *Climate Dyn.*, **16**, 379–392.
- Vimont, D. J., D. S. Battisti, and A. C. Hirst, 2001: Footprinting: A seasonal connection between the Tropics and mid-latitudes. *Geophys. Res. Lett.*, **28**, 3923–3936.
- Vimont D. J., J. M. Wallace, and D. S. Battisti, 2003: The seasonal footprinting mechanism in the Pacific: Implications for ENSO. *J. Climate*, **16**, 2668–2675.
- Vimont, D. J.. 2005: The contribution of the interannual ENSO cycle to the spatial pattern of decadal ENSO-like variability. *J. Climate*, **18**, 2080–2092.
- Weng, W., and J. D. Neelin, 1999: Analytical prototypes for ocean-atmosphere interaction at midlatitudes. Part I: Coupled feedbacks as multiplicative noise stochastic forcing. *J Climate*, **12**, 697–721.

- Winkler, C. R., M. Newman, and P. D. Sardeshmukh, 2001: A linear model of wintertime low-frequency variability. Part I: Formulation and forecast skill. *J. Climate*, **14**, 4474-4494.
- Xie, S.-P., T. Kunitani, A. Kubokawa, M. Nonaka, and S. Hosoda, 2000: Interdecadal thermocline variability in the North Pacific for 1958-97: A GCM simulation. *J. Phys. Oceanogr.*, **30**, 2798-2813.
- Zhang, Y., J. M. Wallace, and D. S. Battisti, 1997: ENSO-like interdecadal variability. *J. Climate*, **10**, 1004–1020.

Table 1. Eigenvalues σ and corresponding e-folding times (eft) of \mathbf{L} . Note that propagating eigenmodes come in complex conjugate pairs; stationary eigenmodes have eigenvalues with zero imaginary parts.

	index	σ_r	σ_i	eft (yr)	
	1	-.062	0	16	
	2	-.170	0	5.9	
	3 (two modes)	-.470	+/- .217	2.1	
	4 (two modes)	-.643	+/- 1.15	1.6	
	5	-.847	0	1.2	
	6	-1.10	0	0.91	
	7 (two modes)	-2.22	+/- 1.49	0.45	

Table 2. IPCC coupled GCMs used in this paper.		
Abbreviation	Model and developer	Length of run (yr)
BCCR	BSM2.0 Bjerknes Centre for Climate Research	250
CCCM	CGCM3.1_T63 Canadian Centre for Climate Modelling and Analysis	300
CNRM	CM3 Centre National de Recherches Meteorologiques (Meteo-France)	250
CSM	CCSM3 National Center for Atmospheric Research (NCAR)-led consortium	500
ECHAM	ECHAM5 Max Planck Institute, Germany	500
ECHO	ECHO-G M&D Group, Max Planck Institute, Germany	500
GFDL-CM2.0	GFDL-CM2.0 NOAA Geophysical Fluid Dynamics Laboratory	500
GFDL-CM2.1	GFDL-CM2.1 NOAA Geophysical Fluid Dynamics Laboratory	500
GISS-AOM	GISS-AOM NASA Goddard Institute for Space Studies	250
GISS/H	GISS-EH NASA Goddard Institute for Space Studies	400
GISS/R	GISS-ER NASA Goddard Institute for Space Studies	500
HADCM3	HadCM3	340

	U. K. Met Office	
HADGEM	HadGEM1 U. K. Met Office	130
IPSL	IPSL-CM4 Institut Pierre Simon Laplace	500
MIROC/ME DRES	MIROC3.2 (medres)	500
MIROC/HIR ES	MIROC3.2 (hires)	100
MRI	MRI-CGCM2.3.2a Meteorological Research Institute, Japan	350
PCM1	PCM1 NCAR & U.S. Department of Energy	500

FIGURES

Fig. 1. Leading EOFs of Tropical SST (left panels) and North Pacific SST (right panels). Contour interval is arbitrary; red shading indicates positive values and blue shading indicates negative values. Also indicated is fraction of variance explained by each EOF for its respective field.

Fig. 2. Local anomaly correlation of SST forecasts for the LIM. Top: One year forecast lead (left) and two year forecast lead (right). Bottom: LIM skill minus skill of persistence forecasts, for forecast leads of one year (left) and two years (right). Contour interval is 0.1 with negative and zero contours indicated by blue shading and dashed lines. Shading of positive values starts at 0.1; redder shading denotes larger values of correlation.

Fig. 3. Cross-validated forecast skill (by PC) for forecast leads of one (blue bars) and two (red bars) years.

Fig. 4. Power spectra for the three leading Tropical PCs (red lines), compared to that predicted by the LIM (blue lines). Gray shading represents the 95% confidence interval determined from a 100000 yr run of the LIM (see text for further details). Thin black solid and dashed lines represent spectra from two different 100-yr periods from the LIM run. The green lines indicate spectra generated by the “fully uncoupled” version of the LIM (i.e., $\mathbf{L}_{NT}=\mathbf{L}_{TN}=0$ and $\langle \boldsymbol{\xi}_N \boldsymbol{\xi}_T^T \rangle = 0$; see section 5). In these log(frequency) versus power times angular frequency (ω) plots, the area under any portion of the curve is equal to the variance within that frequency band.

Fig. 5. Same as Fig. 4 but for the three leading North Pacific PCs.

Fig. 6. Leading empirical normal modes. Contour interval is the same in all panels but is arbitrary. Red shading indicates one sign, and blue shading indicates the other sign.

Fig. 7. Time series ($\alpha_j(t)$) of leading empirical normal modes shown in Fig. 6. Red line in top panel is July-June annual mean GISS global mean surface temperature, scaled to have the same mean and variance as $\alpha_1(t)$ for ease of comparison.

Fig. 8. Cross-validated forecast skill (by empirical eigenmode) for forecast leads of one (top panel) and two (bottom panel) years. Also shown is the predicted skill determined from (7).

Fig. 9. Reconstructed PDO (from second least damped stationary eigenmode \mathbf{u}_2 plus leading propagating eigenmodes \mathbf{u}_3 and \mathbf{u}_4) compared to observed PDO. Red lines indicate times of “regime shifts.”

Fig. 10. (Top) Correlation between “ENSO” (leading Tropical Pacific PC) and “PDO” (leading North Pacific PC) for observations, LIM, LIM with North Pacific forcing of Tropics removed, LIM with Tropics forcing of North Pacific removed, “fully uncoupled” LIM. (Bottom) Coherence between “ENSO” and “PDO” for observations, LIM, LIM with North Pacific forcing of Tropics removed, LIM with Tropics forcing of North Pacific removed, “partially uncoupled” LIM, “fully uncoupled” LIM. Coherence is calculated using the MATLAB “cohere” routine, in which a 10-year Hanning window is applied.

Fig. 11. Propagating eigenmode for the “North Pacific only” linear operator. Top panels: maps corresponding to a phase of $\pi/4$ (left) and $3\pi/4$ (right)); note that this eigenmode has a period of 18.8 yr (phase= 2π). Bottom panels: Hovmoller diagrams showing the evolution of SST along two latitudes: 31°N (left) and 36°N (right). Time increases from bottom to top, showing one complete period with damping excluded. Shading conventions as in Fig. 6.

Fig. 12. Variance of the three leading Tropical PCs from observations and LIM, compared to variances derived from the output of the IPCC coupled GCMs, for (left) annual means and (right) five-year running means. Dark gray bars indicate 95% confidence interval for variance based on 100-yr samples from the LIM.

Fig. 13. Same as Fig. 12 but for the three leading North Pacific PCs.

Fig. 14. Correlation between “ENSO” (leading Tropical Pacific PC) and “PDO” (leading North Pacific PC) for observations, LIM, and IPCC coupled GCMs, for July-June annual means (blue bars) and 5-yr running means (red bars). Green bars indicate 95% confidence interval for PDO-ENSO correlation based on 100-yr samples from the LIM (see text for further details). The correlations for the GISS/AOM model are negative and so are not shown.

Fig. 15. Decorrelation timescales of the projection time series of the leading eigenmodes in observations and in IPCC coupled GCMs.

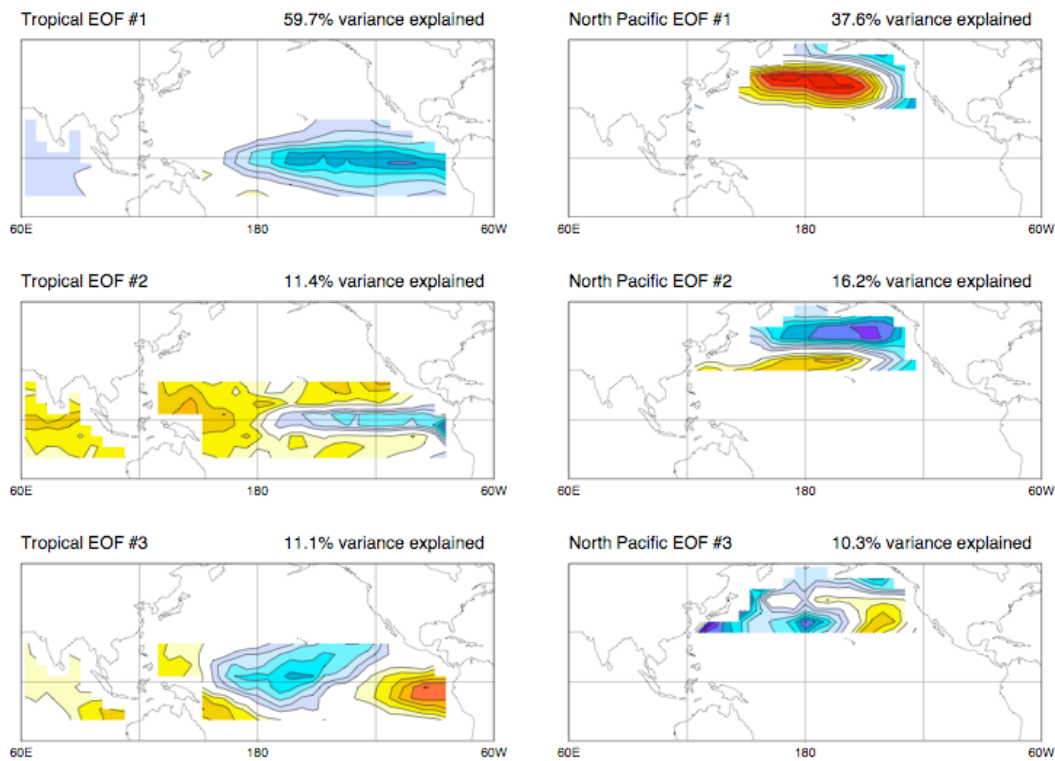


Fig. 1. Leading EOFs of Tropical SST (left panels) and North Pacific SST (right panels). Contour interval is arbitrary; red shading indicates positive values and blue shading indicates negative values. Also indicated is fraction of variance explained by each EOF for its respective field.

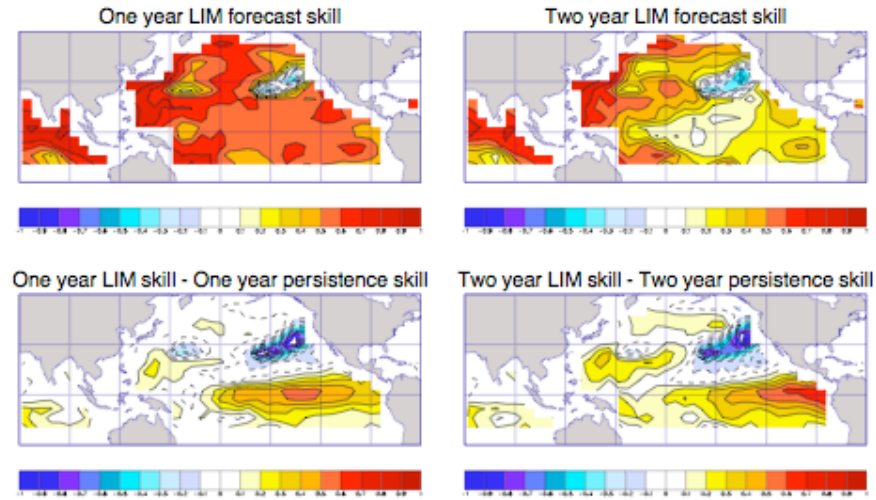


Fig. 2. Local anomaly correlation of SST forecasts for the LIM. Top: One year forecast lead (left) and two year forecast lead (right). Bottom: LIM skill minus skill of persistence forecasts, for forecast leads of one year (left) and two years (right). Contour interval is 0.1 with negative and zero contours indicated by blue shading and dashed lines. Shading of positive values starts at 0.1; redder shading denotes larger values of correlation.

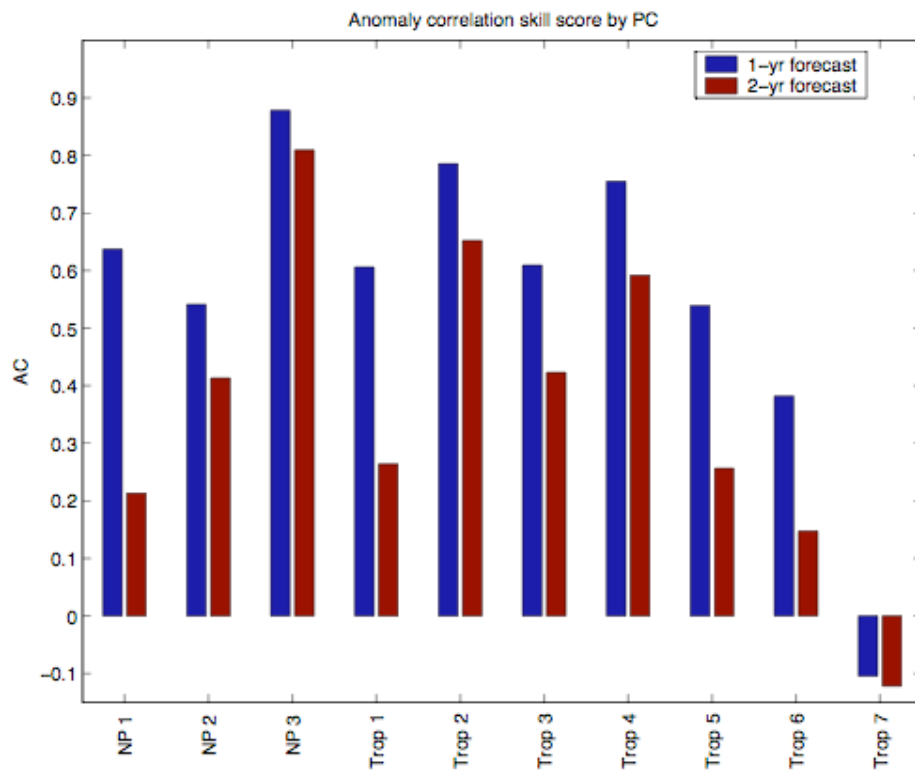


Fig. 3. Cross-validated forecast skill (by PC) for forecast leads of one (blue bars) and two (red bars) years.

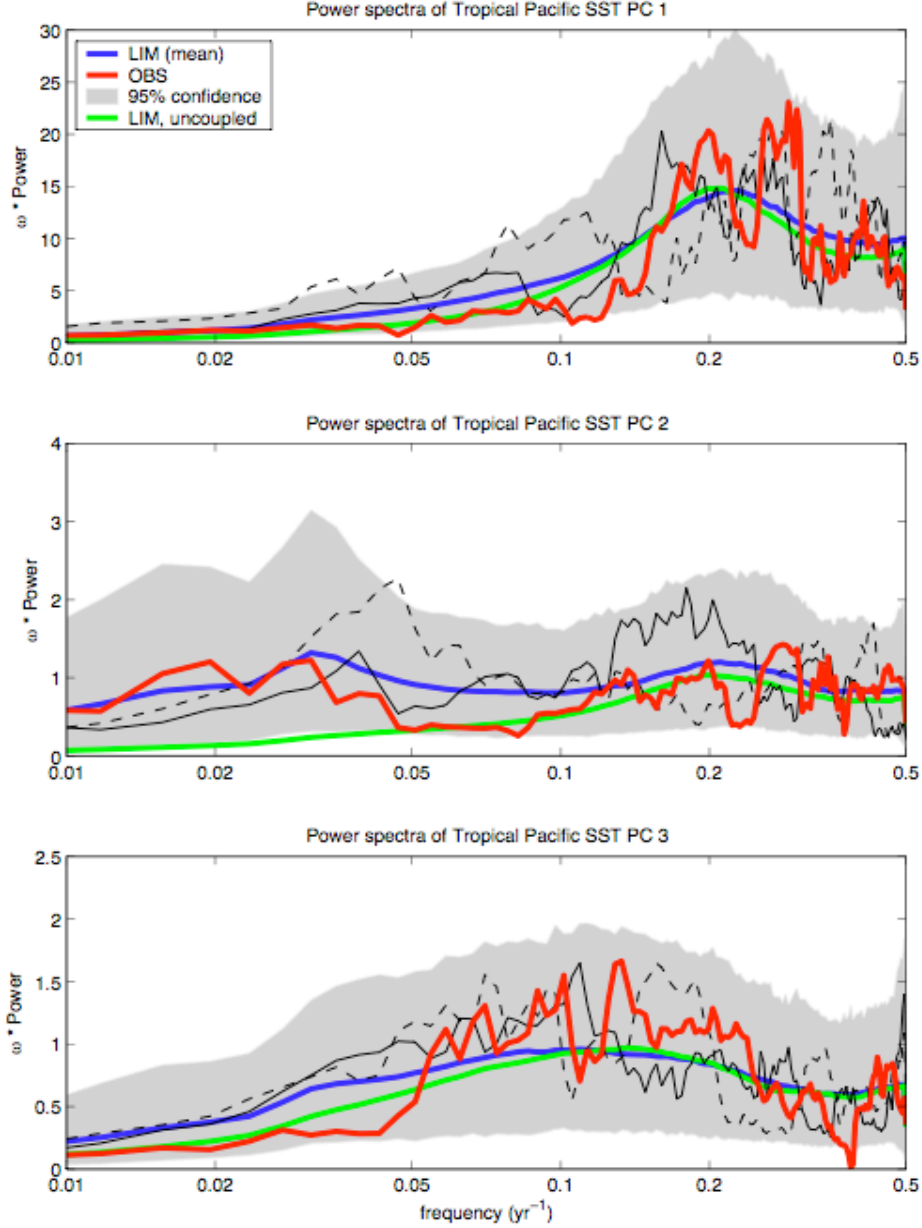


Fig. 4. Power spectra for the three leading Tropical PCs (red lines), compared to that predicted by the LIM (blue lines). Gray shading represents the 95% confidence interval determined from a 100000 yr run of the LIM (see text for further details). Thin black solid and dashed lines represent spectra from two different 100-yr periods from the LIM run. The green lines indicate spectra generated by the “fully uncoupled” version of the LIM (i.e., $\mathbf{L}_{NT}=\mathbf{L}_{TN}=0$ and $\langle \xi_N \xi_T^T \rangle = 0$; see section 5). In these log(frequency) versus power times angular frequency (ω) plots, the area under any portion of the curve is equal to the variance within that frequency band.

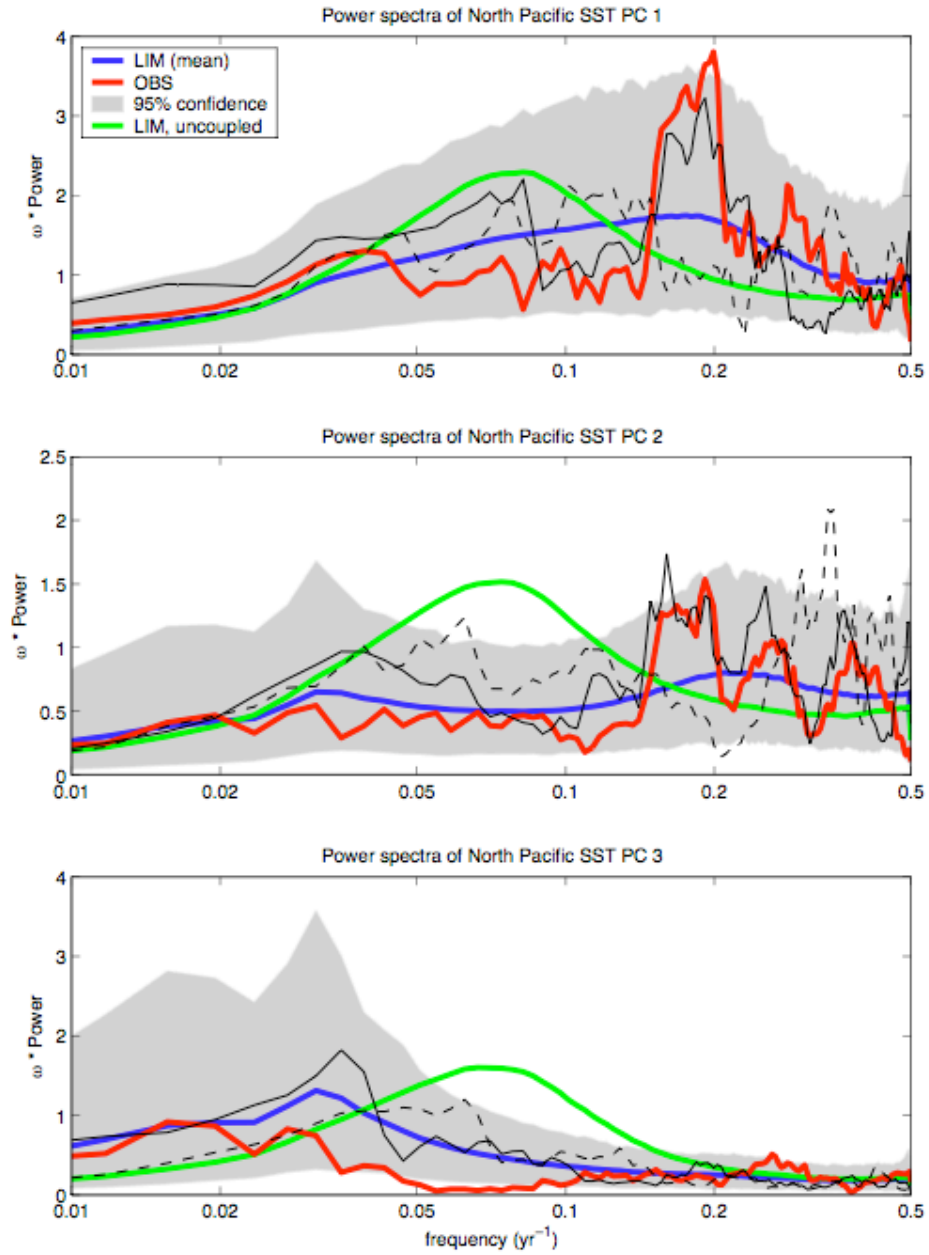


Fig. 5. Same as Fig. 4 but for the three leading North Pacific PCs.

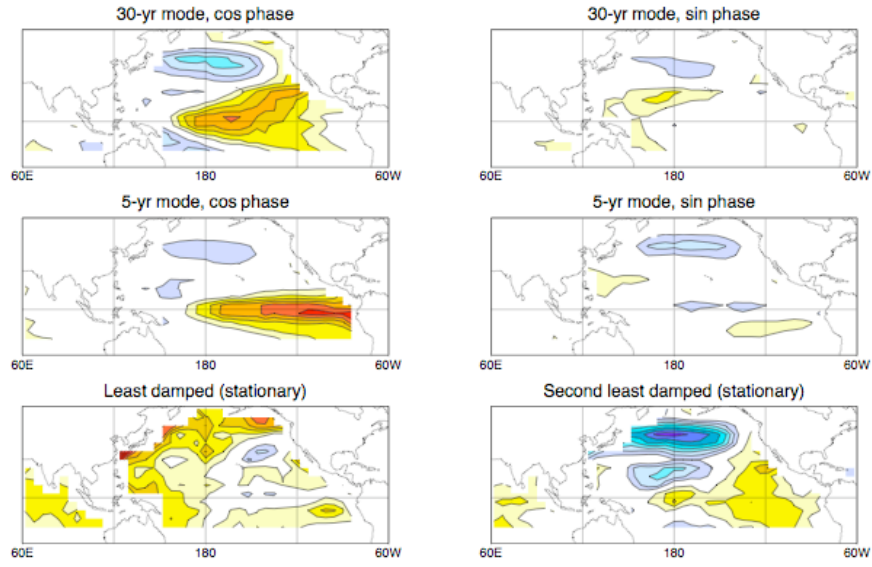


Fig. 6. Leading empirical normal modes. Contour interval is the same in all panels but is arbitrary. Red shading indicates one sign, and blue shading indicates the other sign.

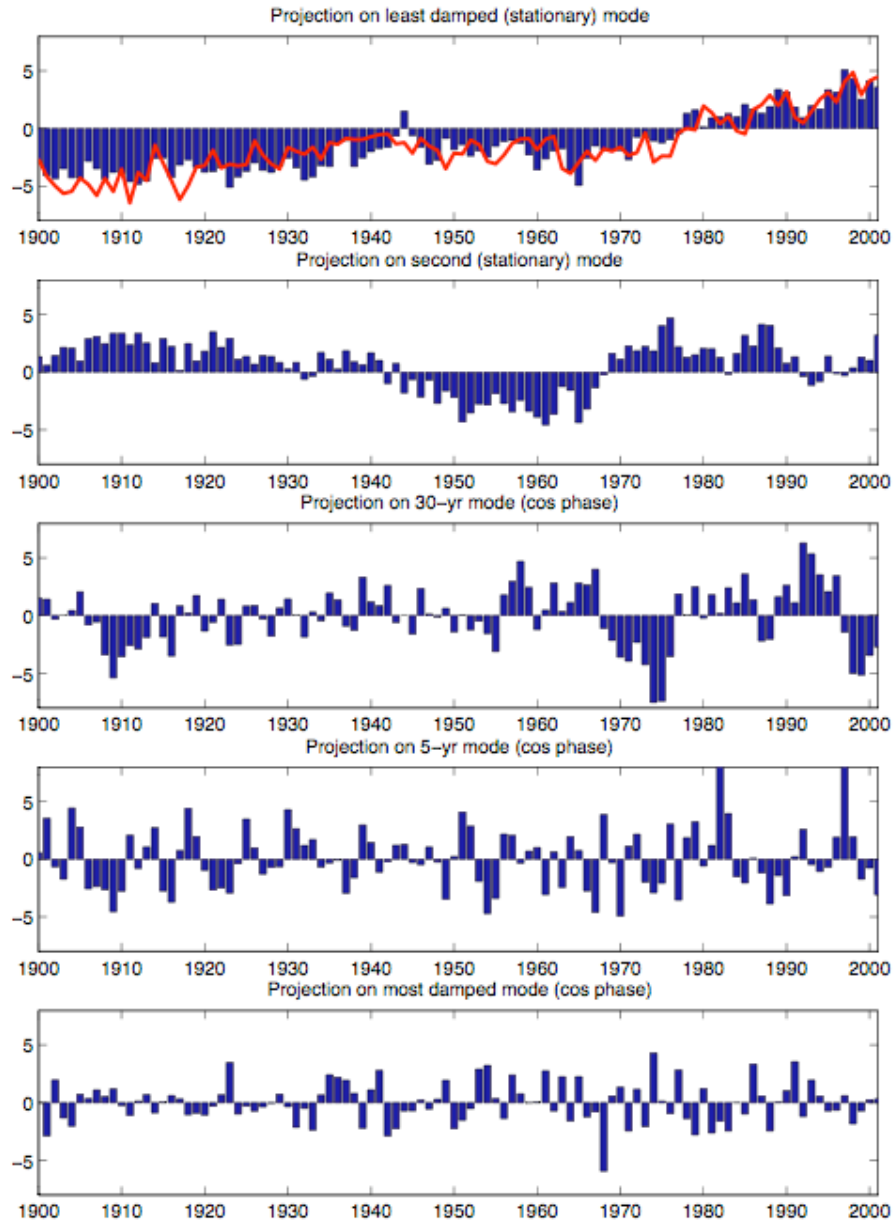


Fig. 7. Time series ($\alpha_j(t)$) of leading empirical normal modes shown in Fig. 6. Red line in top panel is July-June annual mean GISS global mean surface temperature, scaled to have the same mean and variance as $\alpha_j(t)$ for ease of comparison.

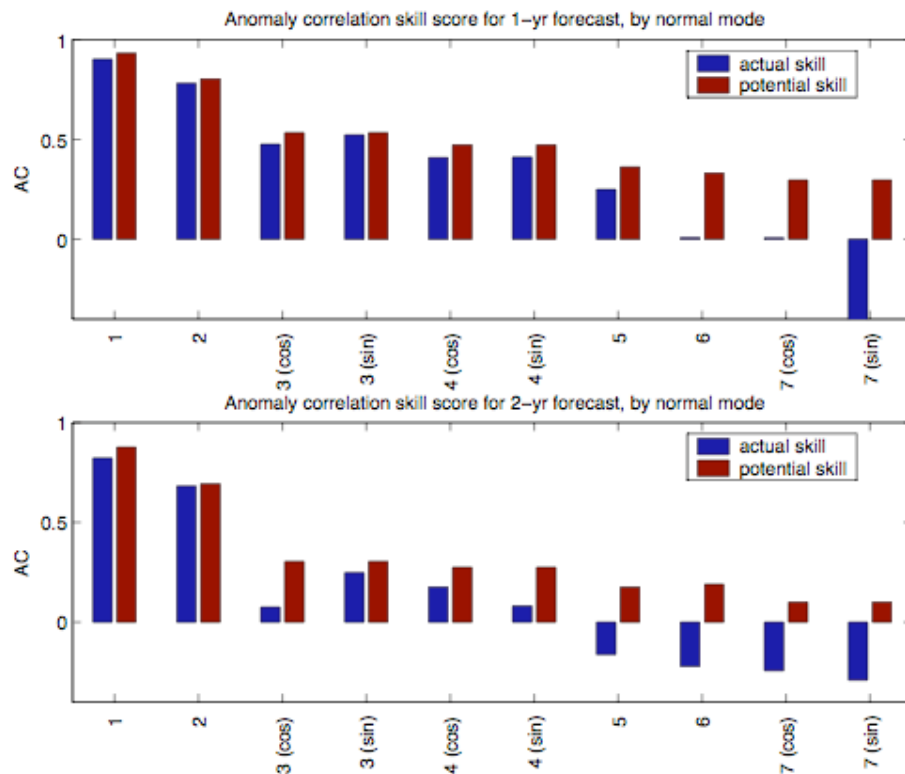


Fig. 8. Cross-validated forecast skill (by empirical eigenmode) for forecast leads of one (top panel) and two (bottom panel) years. Also shown is the predicted skill determined from (7).

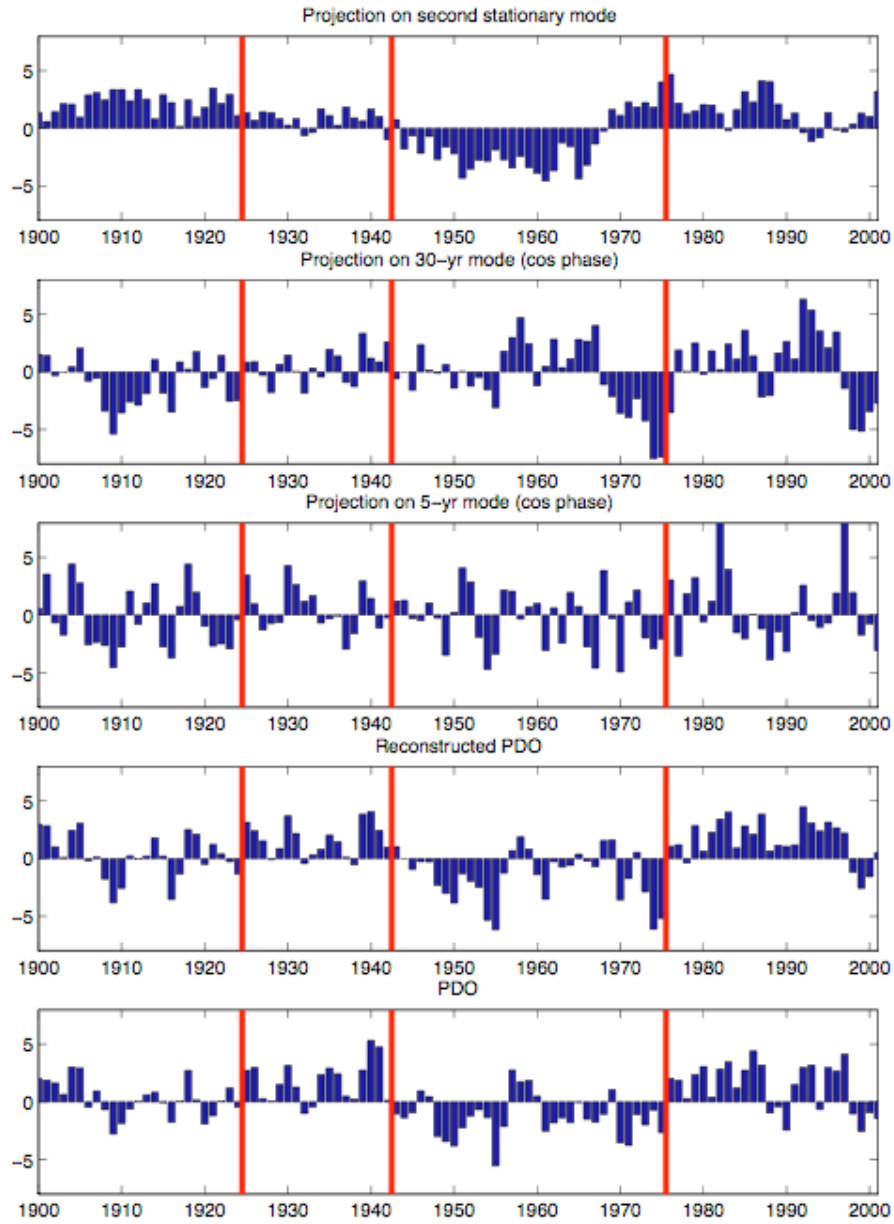


Fig. 9. Reconstructed PDO (from second least damped stationary eigenmode \mathbf{u}_2 plus leading propagating eigenmodes \mathbf{u}_3 and \mathbf{u}_4) compared to observed PDO. Red lines indicate times of “regime shifts.”

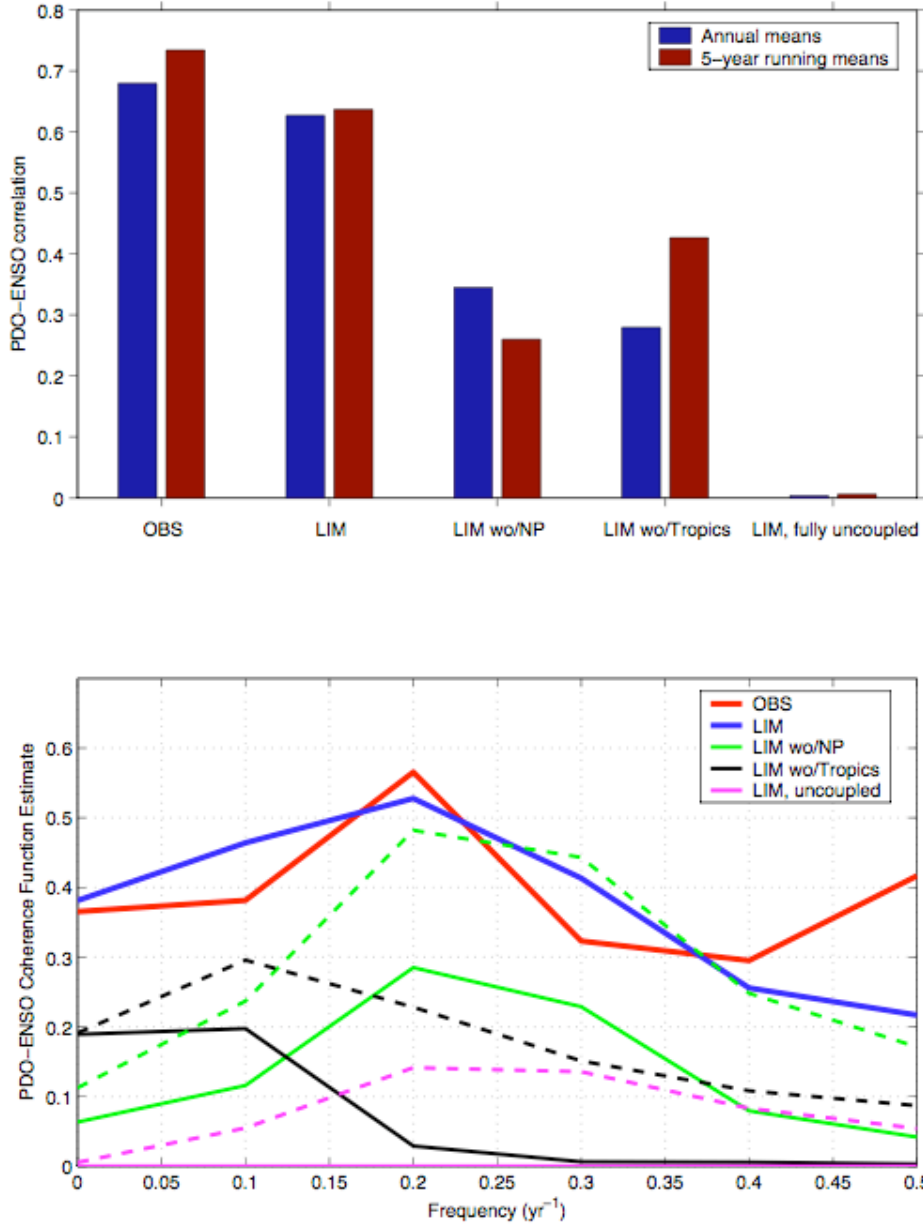


Fig. 10. (a) Correlation between “ENSO” (leading Tropical Pacific PC) and “PDO” (leading North Pacific PC) for observations, LIM, LIM with North Pacific forcing of Tropics removed, LIM with Tropics forcing of North Pacific removed, “fully uncoupled” LIM. (b) Coherence between “ENSO” and “PDO” for observations, LIM, LIM with North Pacific forcing of Tropics removed, LIM with Tropics forcing of North Pacific removed, “partially uncoupled” LIM, “fully uncoupled” LIM. Solid lines indicate runs where correlated noise is removed ($\langle \xi_N \xi_T^T \rangle = 0$), while dashed lines indicate corresponding runs where the noise structure is unaltered. Coherence is calculated using the MATLAB “cohere” routine, in which a 10-year Hanning window is applied.

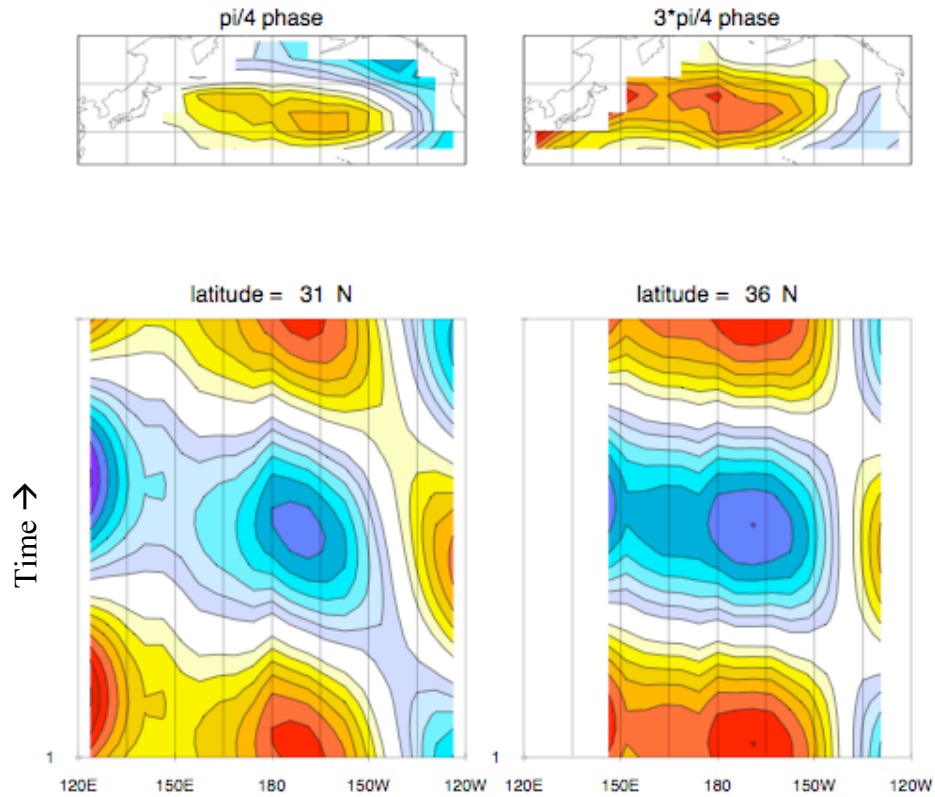
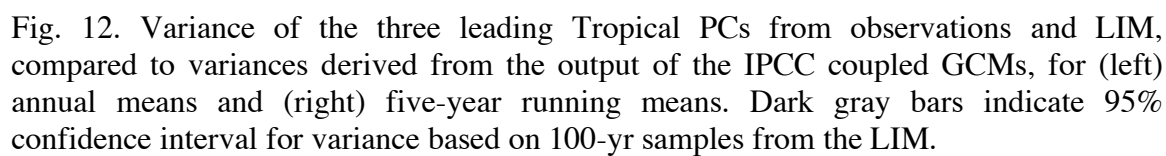


Fig. 11. Propagating eigenmode for the “North Pacific only” linear operator. Top panels: maps corresponding to a phase of $\pi/4$ (left) and $3\pi/4$ (right); note that this eigenmode has a period of 18.8 yr (phase= 2π). Bottom panels: Hovmöller diagrams showing the evolution of SST along two latitudes: 31°N (left) and 36°N (right). Time increases from bottom to top, showing one complete period with damping excluded. Shading conventions as in Fig. 6.

Decadal variability



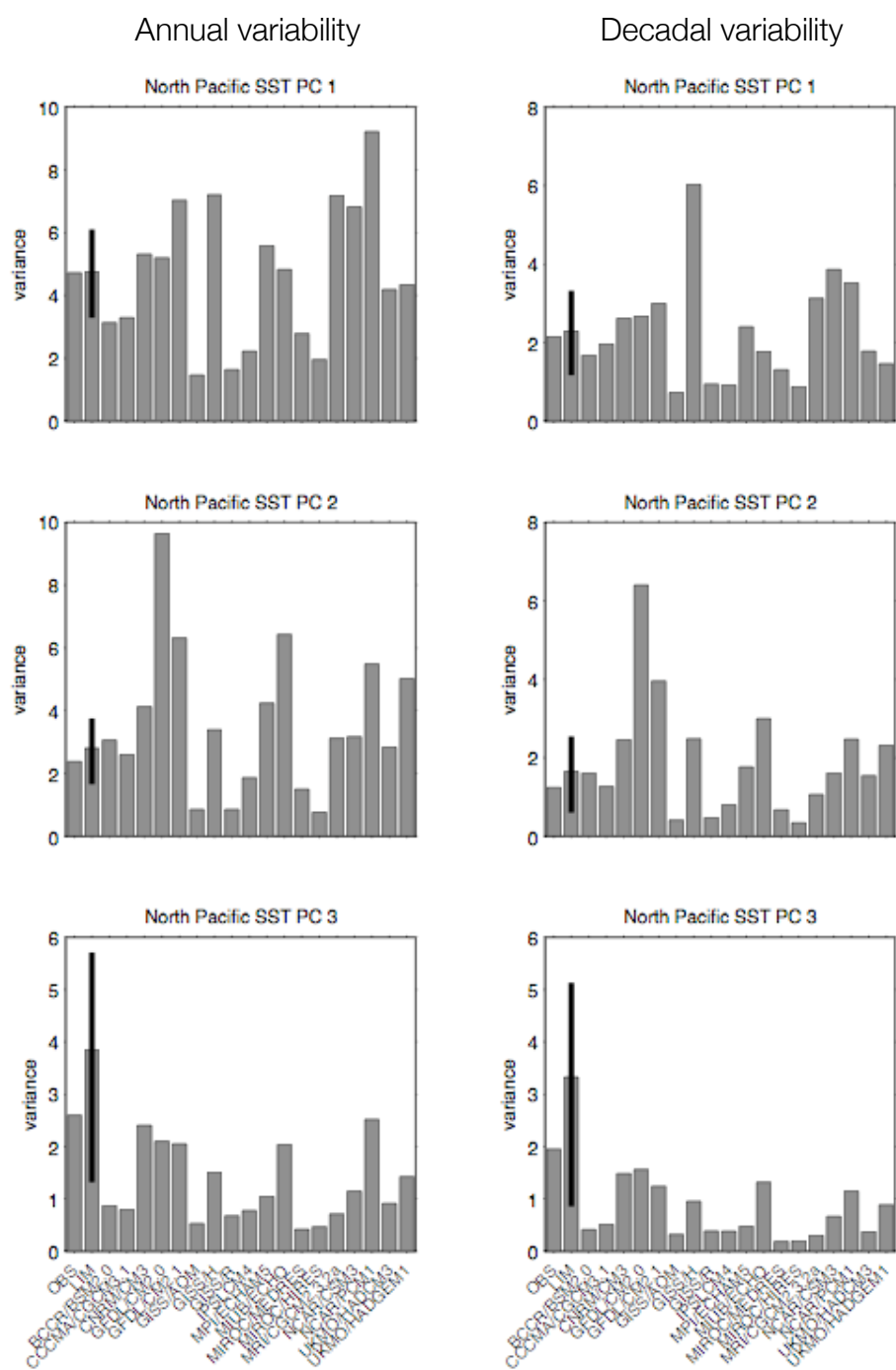


Fig. 13. Same as Fig. 12 but for the three leading North Pacific PCs.

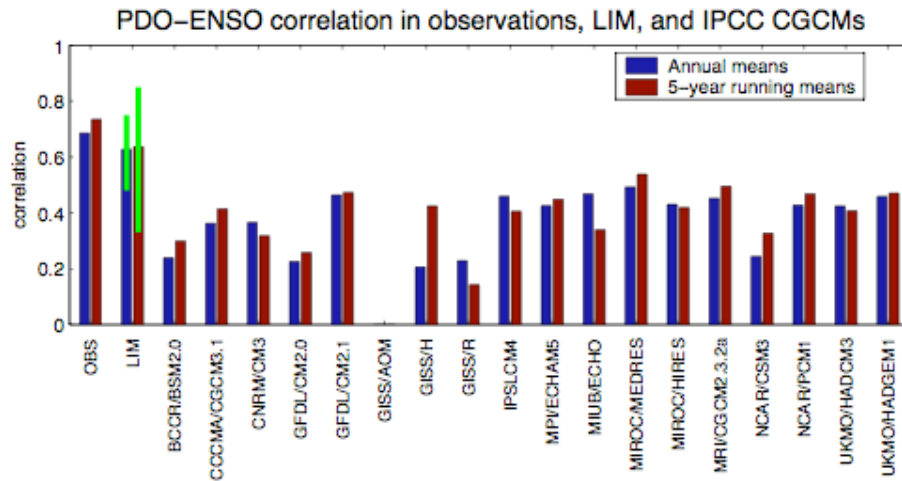


Fig. 14. Correlation between “ENSO” (leading Tropical Pacific PC) and “PDO” (leading North Pacific PC) for observations, LIM, and IPCC coupled GCMs, for July-June annual means (blue bars) and 5-yr running means (red bars). Green bars indicate 95% confidence interval for PDO-ENSO correlation based on 100-yr samples from the LIM (see text for further details). The correlations for the GISS/AOM model are negative and so are not shown.

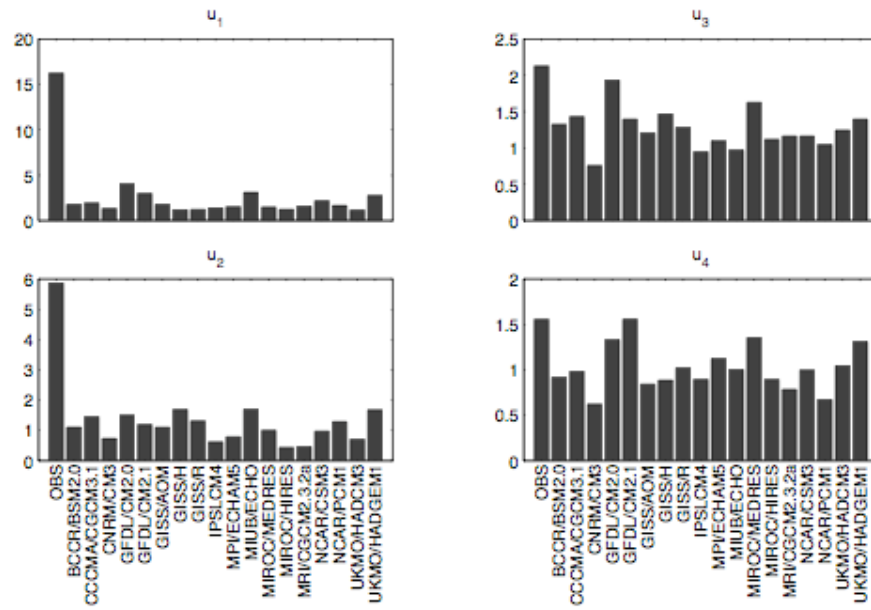


Fig. 15. Decorrelation timescales of the projection time series of the leading eigenmodes in observations and in IPCC coupled GCMs.